

N=4 SYM and QCD motivated approach to soft interactions at high energies

E. Gotsman^{a*}, E. Levin^{a,b†} and U. Maor^{a‡}

a) Department of Particle Physics, School of Physics and Astronomy, Raymond and Beverly Sackler Faculty of Exact Science, Tel Aviv University, Tel Aviv, 69978, Israel

b) Departamento de Física, Universidad Técnica Federico Santa María, Avda. España 1680, Casilla 110-V, Valparaíso, Chile

ABSTRACT: In this paper we construct a model that satisfies the theoretical requisites of high energy soft interactions, based on two ingredients: (i) the results of N=4 SYM, which at present is a unique theory that allows one to deal with a large coupling constant; and (ii) the requirement of matching with high energy QCD. In accordance with these ideas, we assume that the soft Pomeron intercept is rather large, and the slope of the Pomeron trajectory is equal to zero. We derive analytical formulae that sum both enhanced and semi-enhanced diagrams for elastic and diffractive amplitudes. We fit the available experimental data, and predict the value for cross sections at the energies accessible at the LHC. The main corrections to the model are studied and evaluated.

KEYWORDS: Soft Pomeron, BFKL Pomeron, Diffractive Cross Sections, N=4 SYM.

PACS: 13.85.-t, 13.85.Hd, 11.55.-m, 11.55.Bq

*Email: gotsman@post.tau.ac.il.

†Email: leving@post.tau.ac.il

‡Email: maor@post.tau.ac.il.

1. Introduction	2
1.1 N=4 SYM	2
1.2 Matching with perturbative QCD	3
1.3 Models of high energy soft interaction	4
2. Main ideas and assumptions	5
2.1 Soft Pomeron	5
2.2 $\alpha'_{\mathbb{P}} = 0$	5
2.3 Good-Walker mechanism	6
2.4 Pomeron -Pomeron vertices	7
2.5 The phenomenological parameters and their typical values	9
3. Summing the enhanced diagram	10
3.1 Improved MPSI approximation	10
3.2 The range of energy for which our approach is reliable	12
3.3 The Pomeron Green's function and the elastic scattering amplitude	13
3.4 The exact vertex and diffractive production	14
4. Summing the full set of diagrams	15
4.1 Elastic scattering	15
4.2 Diffractive production	18
5. Corrections to our approach	22
5.1 $\alpha'_{\mathbb{P}} \neq 0$ and the Pomeron as a fixed branch point	22
5.2 Low energy description and the 'threshold effect'.	25
5.2.1 Low energy behaviour of the scattering amplitude	25
5.2.2 The 'threshold' effect	26

6. The fit to the data and its phenomenology	27
6.1 The main formulae of the fit	27
6.2 The strategy of our fitting procedure	28
6.3 The results of the fit	28
6.4 Comments on the parameter values of the fit	29
6.5 Comparison with other approaches.	30
7. Conclusions	32

1. Introduction

Thanks to the hard work of experimentalists and theoreticians over the past four decades, we know that the most economical and reliable method for describing soft interactions at high energy, is the phenomenology based on the soft Pomeron and secondary Reggeons (see Refs. [1–3] for details). Consequently, we believe that the future theory should be a theory of Pomeron and Reggeons and their interactions. However, numerous attempts [2, 4] to build such a theory have failed, as one was not able to specify the Pomeron interaction, as well as interaction of Pomerons with the target. We are doomed to make *ad hoc* assumptions about the vertices of multi-Pomeron interactions (see Ref. [4–6, 9, 10]) which specify the approach, but do not make it more theoretically reliable. Such assumptions seem unavoidable, as there is no theoretical approach to non-perturbative QCD and, on the other hand, soft high energy processes appear to be typical examples of non-perturbative physics at long distances. These processes are even more difficult to calculate, as approximate methods such as QCD sum rules and/or effective theories, as well as the lattice QCD approach, cannot be employed to determine the high energy amplitudes. The success of any phenomenology does not establish a theory, however over the past two years a new approach has been developed (N=4 SYM), which allows one to study theoretically the regime of the strong coupling constant [11].

1.1 N=4 SYM

We use this theory as a guide for the physics phenomena occurring in this regime. The attractive feature of this theory is that N=4 SYM with small coupling, leads to normal QCD like physics (see Refs. [12, 13]), with OPE and linear equations for DIS, as well as the BFKL equation for the high energy amplitude. The high energy amplitude reaches the unitarity limit: black disc regime, in which half of the cross section stems from elastic scattering, and half relates to processes of multiparticle production.

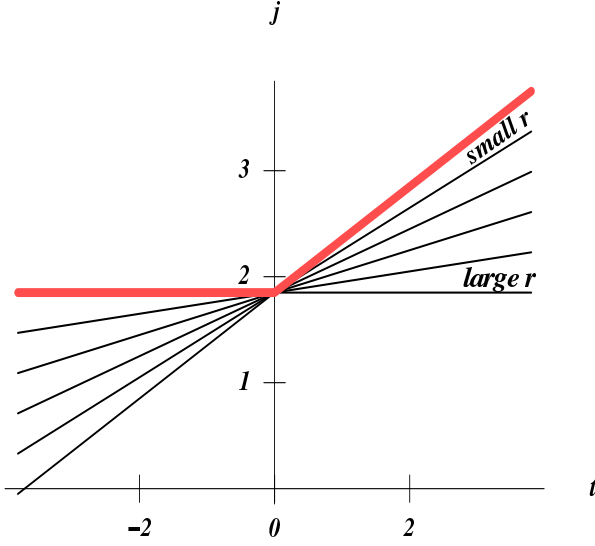


Figure 1: The behaviour of the Pomeron trajectory in N=4 SYM according to Ref. [14]. The figure is taken from Ref. [14]

On the other hand, making use of the fact that with the aid of the AdS/CFT correspondence [11] this theory can be solved analytically, and can be reduced to weak gravity in AdS_5 space.

the resonance region of positive t ; and (iv) the Pomerons (gravitons) interact by means of the triple Pomeron vertex which is small (at least $\propto 2/\sqrt{\lambda}$). The minute value of α'_P is not related to the small size of the partons in this theory. It is related to small values of the fifth coordinate r (see Fig. 1). The physical meaning of this coordinate is, related to the typical size of the colliding particles. It should be stressed that all these features are an integral part of the theory and therefore, for the first time we have theoretical justification for using Reggeon-type phenomenology in high energy scattering.

In this paper we present our approach based on two major assumptions: it reproduces the main features of N=4 SYM, and it provides a natural matching with the perturbative QCD approach. For the sake of completeness we discuss the perturbative approach below.

1.2 Matching with perturbative QCD

In perturbative QCD the high energy amplitude has been calculated in the leading log approximation, in which $\alpha_S \ll 1$ but $\alpha_S \log s \approx 1$, where $\sqrt{s} = W$ denotes the energy in the c.m. frame [22–24]. This amplitude can be written as the exchange of the BFKL Pomeron [23], which has the following form for the cross section for the scattering of one colourless dipole of size r on another dipole of size R

$$\sigma(r, R; s) = \int d^2b d^2\rho_1 d^2\rho_2 \int_{-i\infty+\epsilon}^{+i\infty+\epsilon} \frac{d\nu}{2\pi i} V(r, \rho_1; \nu) e^{\omega(\nu)Y} V(R, \rho_2; -\nu) \delta^{(2)}(\rho_1 - \rho_2 - b) \quad (1.1) \quad \boxed{\text{I2}}$$

where

$$\omega(\nu) = \alpha_S (2\psi(1) - \psi(1/2 + i\nu) - \psi(1/2 - i\nu)) \quad (1.2) \quad \boxed{\text{I3}}$$

and $\psi(z) = d \log \Gamma(z)$, and $\Gamma(z)$ is the Euler gamma function.

One can see that the BFKL Pomeron is not a pole in angular momentum, but it is a cut. However, at fixed ν which is the conjugate variable to $\ln(r^2/R^2)$, it is a pole. The position of this pole does not depend on momentum transfer (or b) and, therefore, the corresponding α' is equal to zero.

It turns out that in the wide range of energy $1/\alpha_S^2 \gg \ln s \gg 1$ the scattering amplitude can be expressed as the sum of BFKL Pomeron exchanges and their interactions (see Refs. [25–32]. Perturbative QCD specifies the Pomeron vertices, and in the LO approach, the only vertex that contributes is the triple BFKL Pomeron vertex [31, 32].

1.3 Models of high energy soft interaction

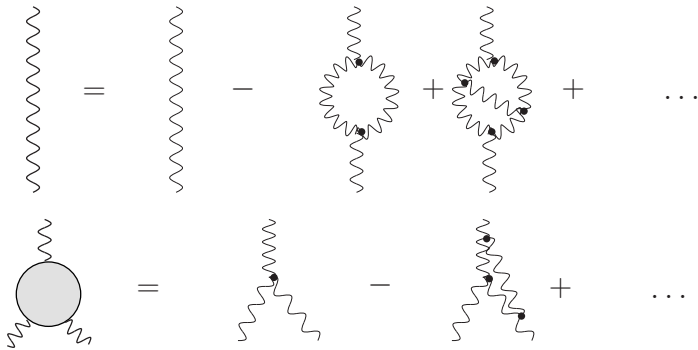


Figure 2: The exact Green's function of the Pomeron as a sum of enhanced diagrams and the exact triple Pomeron vertex.

We are incapable of building a theory of high energy scattering, as the problem of the confinement of quarks and gluons in QCD has not been solved, and we do not have a theoretical tool for describing the interactions of quarks and gluons at long distances. Therefore, we are doomed to build models that take into account our ideas of the behaviour of QCD at long distances. We believe that such models should include everything that we know about QCD at long distances and, in particular, should

absorb all that we have learned about high energy scattering in N=4 SYM. We can summarize this knowledge as a list of criteria that a model should satisfy, namely,

1. The model should be built using Pomerons and Reggeons as the main ingredients;
2. The intercept of the Pomeron should be rather large. In N=4 SYM we expect $\Delta_P = \alpha_P(0) - 1 = 1 - 2/\sqrt{\lambda} \approx 0.3 \div 0.4$, since the estimate for λ from the cross section for multiparticle production as well as from DIS at HERA [33] is $\lambda = 5 \div 9$;
3. $\alpha'_P(0) = 0$;
4. A large contribution should come from processes of diffraction dissociation, since in N=4 SYM at large λ only these processes contribute to the scattering amplitude. In other words, the model should include the Good-Walker mechanism [45] as the main source of the diffraction production;
5. The Pomeron self-interaction should be small (of the order of $2/\sqrt{\lambda}$ in N=4 SYM), and much smaller than the vertex of interaction of the Pomeron with a hadron, which is of the order of λ ;
6. The last requirement follows not from N=4 SYM, but from the natural matching with perturbative QCD: where the only vertex that contributes is the triple Pomeron vertex.

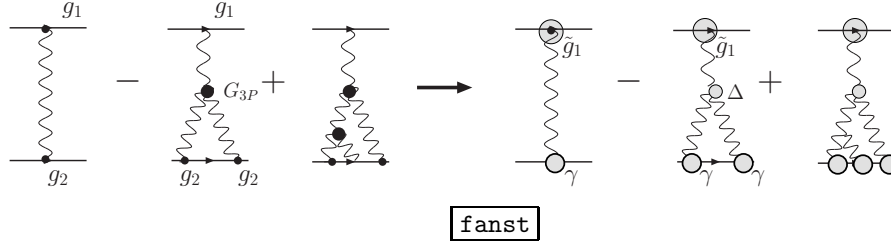


Figure 3: Examples of 'fan' Pomeron diagrams: in Reggeon Calculus (the first three diagrams) and in the generating function approach (the last three).

In this paper we continue to develop a model that satisfies all above criteria. In our previous paper (see Ref [7]) we suggested a model that includes the large diffraction from Good-Walker mechanism and a Green's function of the Pomeron that sums all enhanced diagrams (see Fig. 2). However, we neglected the contribution of other Pomeron diagrams (see for example the so called fan diagrams in Fig. 3). The line of argument for justifying this was the following: The value of the triple Pomeron vertex turns out to be small, and the cross section for the diffraction production in the region of large mass makes up 10 - 20% of total cross section of the diffractive production. Therefore, we decided in the first approximation to neglect the process of diffraction of large masses, and calculate them perturbatively. In this paper we sum all 'fan' diagrams together with the enhanced ones.

2. Main ideas and assumptions

2.1 Soft Pomeron

As we have mentioned we wish to suggest a procedure which contains the main features of N=4 SYM, and provides a transparent matching with perturbative QCD, which plays the role of the correspondence principle in our approach.

The good news is that the soft Pomeron is a natural ingredient in N=4 SYM. Actually, in N=4 SYM we have an infinite series of different Regge poles (see Fig. 1). Our simplification is to replace this set of poles by one pole: the Pomeron, shown in Fig. 1 in red. We feel confident with the assumption regarding the existence of the soft Pomeron, since it has been successfully utilized in high energy phenomenology for the last forty years, and it appears in QCD (see above).

From N=4 SYM we expect that the value of $\Delta = \alpha_P(0) - 1 = 1 - 2/\sqrt{\lambda}$ could be large.

2.2 $\alpha'_P = 0$

Our second ingredient is that the slope of the Pomeron $\alpha'_P = 0$. As we have discussed, $\alpha'_P = 0$ is in perfect agreement with N=4 SYM predictions. It also agrees with the recent fit to high energy data [7]. This fact might appear strange, as for a long time the widely accepted value for α'_P was $\alpha'_P = 0.25 \text{ GeV}^{-2}$ [43]. Comparing with the parametrization of Ref. [43], two new ingredients have been introduced: a large value

of $\Delta \approx 0.3$ instead of $\Delta \approx 0.08$ in Ref. [43], and sufficiently large shadowing corrections, which were considered small in Ref. [43].

We believe that a small value of $\alpha'_{\mathcal{P}}$, is a signal that rather short distances contribute to the soft interaction at high energy, in agreement with all approaches to the Pomeron structure considered above.

It should be stressed that N=4 SYM gives a new possibility for high energy asymptotic behaviour: a Regge cut (Pomeron) that does not move in the scattering region, while it has a slope $\alpha'_{\mathcal{P}}$ in the region of positive t . In Ref. [44] such a possibility was missed. It is interesting to note that in N=4 SYM this property of the Pomeron (graviton) contribution, stems from the integration over the fifth coordinate z , which has the meaning of integration over the possible size of the hadrons.

2.3 Good-Walker mechanism

The third conclusion that we derive from N=4 SYM, is the large contribution of the diffractive dissociation processes. In our approach the diffraction dissociation is taken into account using the two channel model which we have developed in a number of papers (see Ref. [7] and references therein). In this formalism, diffractively produced hadrons at a given vertex are considered as a single hadronic state described by the wave function Ψ_D , which is orthonormal to the wave function Ψ_h of the incoming hadron (proton in the case of interest), $\langle \Psi_h | \Psi_D \rangle = 0$. We introduce two wave functions ψ_1 and ψ_2 which diagonalize the 2x2 interaction matrix \mathbf{T}

$$A_{i,k} = \langle \psi_i | \psi_k | \mathbf{T} | \psi_{i'} | \psi_{k'} \rangle = A_{i,k} \delta_{i,i'} \delta_{k,k'}. \quad (2.1) \quad \boxed{2\text{CHM}}$$

In this representation the observed states are written in the form

$$\psi_h = \alpha \psi_1 + \beta \psi_2, \quad (2.2) \quad \boxed{2\text{CHM31}}$$

$$\psi_D = -\beta \psi_1 + \alpha \psi_2, \quad (2.3) \quad \boxed{2\text{CHM32}}$$

where, $\alpha^2 + \beta^2 = 1$. Using Eq. $\boxed{2\text{CHM}}$, we can rewrite the unitarity constraints in the form

$$\text{Im } A_{i,k}(s, b) = |A_{i,k}(s, b)|^2 + G_{i,k}^{\text{in}}(s, b), \quad (2.4) \quad \boxed{\text{UNIT}}$$

where $G_{i,k}^{\text{in}}$ is the contribution of all non diffractive inelastic processes, i.e. it is the summed probability for these final states to be produced in the scattering of particle i off particle k .

A simple solution of Eq. $\boxed{2.4}$ has the same structure as in the single channel formalism,

$$A_{i,k}(s, b) = i \left(1 - \exp \left(-\frac{\Omega_{i,k}(s, b)}{2} \right) \right), \quad (2.5) \quad \boxed{2\text{CHM1}}$$

$$G_{i,k}^{\text{in}}(s, b) = 1 - \exp(-\Omega_{i,k}(s, b)). \quad (2.6) \quad \boxed{2\text{CHM2}}$$

From Eq. $\boxed{2.6}$ we deduce, that the probability that the initial projectiles (i, k) reach the final state interaction unchanged, regardless of the initial state rescatterings, is $P_{i,k}^S = \exp(-\Omega_{i,k}(s, b))$.

The opacities $\Omega_{i,k}(s, b)$ have to be determined and we will discuss this below. In general this two channel approach is a particular case of the Good-Walker mechanism [45] for diffractive production, and

we can account for diffraction in the region of small mass using this approach. For the region of large values of produced mass in diffractive dissociation, it is necessary to develop a theoretical approach to the Pomeron-Pomeron interaction.

2.4 Pomeron -Pomeron vertices

The general framework for accounting for Pomeron interactions was developed in 70's (see Refs. [2, 46] in the framework of Reggeon Calculus. However, being purely phenomenological, Reggeon Calculus is not able to fix the vertices of Pomeron interactions. The values of vertices, and their number, have to be introduced in Reggeon Calculus from the microscopic theory.

Our third ingredient is the assumption that only the triple Pomeron vertex is essential. This assumption is in full agreement with N=4 SYM and perturbative QCD: in both these theoretical approaches only this vertex contributes. We consider this to be essential, as this assumption provides a natural bridge to perturbative QCD. To illustrate this matching we consider the sum of the ‘fan’ Pomeron diagrams (see Fig. ^{fanst}₃).

Instead of the generating functional for high density QCD (see Ref. [36]), we can introduce the generating function:

$$Z(Y - Y_0; u) = \sum_{n=1}^{\infty} P_n(Y - Y_0) u^n \quad (2.7) \quad \boxed{\text{ZF}}$$

where $P_n(Y - Y_0)$ is the probability to find n -Pomerons at rapidity $Y - Y_0$. By fixing the size of the interacting dipoles, one can see that Eq. (2.7) differs from the generating functional in the dipole approach of high density QCD.

The full set of the ‘fan’ diagrams can be summed using the following equation for the generating function

$$\frac{\partial Z(Y - Y_0; u)}{\partial Y} = -\Delta u(1 - u) Z(Y - Y_0; u) \quad (2.8) \quad \boxed{\text{ZFEQ}}$$

with the amplitude that is given by the following equation

$$N(Y; \{\gamma_i\}) = -\sum_{n=1}^{\infty} \int \gamma_n(Y_0) \prod_{i=1}^n \frac{\partial^i}{\partial u^i} Z(Y, u)|_{u=1} = -\sum_{n=1}^{\infty} (-1)^n \gamma_n(Y_0) \rho(Y - Y_0) \quad (2.9) \quad \boxed{\text{NF}}$$

If we neglect dependence on the size of the dipoles, then both equations coincide with the equation in the dipole approach to QCD. These equations sum the set of ‘fan’ diagrams, if we replace (see Fig. ^{fanst}₃)

$$g_1 \rightarrow \tilde{g}_1 = \frac{g_1 \Delta}{G_{3P}}; \quad G_{3P} \rightarrow \Delta; \quad g_2 \rightarrow \gamma = \frac{G_{3P} g_2}{\Delta} \quad (2.10) \quad \boxed{\text{REP}}$$

where Δ denotes the intercept of the Pomeron, and γ the amplitude of the interaction of the ‘wee’ parton (colorless dipole) with the target. The scattering amplitude is equal to $\tilde{g}_1 N(Eq. (\text{2.9})^{\text{NF}})$.

Assuming that only the triple Pomeron vertex is essential, we achieve the matching between perturbative QCD and our approach. We will show below that this matching can be demonstrated for sets of Pomeron diagrams, more complicated than the ‘fan’ diagrams.

The theory that includes all the ingredients that have been discussed above, can be formulated in a functional integral form [31],

$$Z[\Phi, \Phi^+] = \int D\Phi D\Phi^+ e^S \quad \text{with } S = S_0 + S_I + S_E, \quad (2.11)$$

where S_0 describes the free Pomerons, S_I corresponds to their mutual interaction, and S_E relates to the interaction with the external sources (target and projectile). Since $\alpha'_P = 0$, S_0 has the form

$$S_0 = \int dY \Phi^+(Y) \left\{ -\frac{d}{dY} + \Delta \right\} \Phi(Y). \quad (2.12) \quad \boxed{\text{S0}}$$

S_I includes only triple Pomeron interactions and is of the form

$$S_I = g_{3P} \int dY \{ \Phi(Y) \Phi^+(Y) \Phi^+(Y) + h.c. \} \quad (2.13) \quad \boxed{\text{SI}}$$

S_E depends on our model for the interaction of the Pomeron with the scattering particles, which we will specify later.

This theory, as any theory of Pomeron interactions, is written in such a way that the high energy amplitudes satisfy t -channel unitarity. However, s -channel unitarity remains a problem. In Refs. [37] it was shown that to satisfy s -channel unitarity we need to add to the interaction term (S_I), the four Pomeron vertex $-\Gamma(2 \rightarrow 1)(\Phi^+)^2(\Phi)^2$.

For a better understanding of s -channel unitarity we reformulate the theory, given by the functional integral of Eq. (2.11), in terms of the evolution equations for the system of partons. As we have mentioned, for perturbative QCD these partons are colourless dipoles, as was shown in Ref. [34], that can decay and merge: one parton to two partons and two partons into one parton, with probabilities $\Gamma(1 \rightarrow 2)$ and $\Gamma(2 \rightarrow 1)$ respectively. For such a system of partons, we can write a simple evolution equation (Fokker-Planck equation). Indeed, let $P_n(y)$ be the probability to find n -parton (dipoles) with rapidity y in the wave function of the fastest (parent) parton (dipole), moving with rapidity $Y > y$. For $P_n(y)$, we write down a recurrence equation (see Refs. [36, 48])

$$-\frac{\partial P_n(y)}{\partial y} = \Gamma(1 \rightarrow 2) \{ -n P_n + (n-1) P_{n-1} \} + \Gamma(2 \rightarrow 1) \{ -n(n-1) P_n + (n+1)n P_{n+1} \}. \quad (2.14) \quad \boxed{\text{PNEQ}}$$

In each bracket the first term on the r.h.s., can be viewed as a probability of a dipole annihilation in the rapidity range (y to $y - dy$) (death term). The second is a probability to create one extra dipole (birth term). Note the negative sign in front of $\partial P_n(y)/\partial y$. It appears due to our choice of the rapidity evolution, which starts at the largest rapidity $y = Y$, of the fastest dipole and then decreases. The first two terms are responsible for the process of parton decay, while the last two terms describe the contribution of partons merging.

Using Eq. (2.7) we can re-write Eq. (2.14) in the form

$$-\frac{\partial Z(y, u)}{\partial y} = -\kappa u(1-u) \frac{\partial Z(y, u)}{\partial u} + u(1-u) \frac{\partial^2 Z(y, u)}{\partial^2 u}. \quad (2.15) \quad \boxed{\text{GFEQ}}$$

where $\mathcal{Y} \equiv \Gamma(2 \rightarrow 1)(Y - y) = \Delta \gamma(Y - y)$ and $\kappa \equiv 1/\gamma$.

Eq. (2.15)^[GFEQ] should be added with the initial condition at $Y = Y_0$, as well as the boundary condition

$$Z(y, u = 1) = 1, \quad (2.16) \quad \boxed{\text{INC2}}$$

which follows from the physical meaning of P_n as a probability. It turns out that Eq. (2.15)^[GFEQ] can be solved analytically with an arbitrary initial condition [49, 50]. Therefore, formally speaking we could derive the initial condition for different processes and obtain the solution using the approach of Ref. [50]. However, we chose a different and more traditional way to tackle the problem. As was suggested in Ref. [46] the solution of the Pomeron interaction problem should have two steps. Step one, is to find the correct Green's function of the Pomeron, and the exact vertex of the triple Pomeron interaction, by summing all enhanced diagrams (see Fig. 2)^[enhst]. Step two: to solve the problem of the interaction of new (exact) Pomerons. One expects that the interaction in terms of the exact Green's function and vertices, will be much simpler at high energy, as the main effect of the interaction has been taken into account in step one.

It is necessary to require that there be only one fastest parton (dipole), which is $P_1(y = Y) = 1$, while $P_{n>1}(y = Y) = 0$. In this case we have the following initial condition for the generating function

$$Z(y = Y) = u. \quad (2.17) \quad \boxed{\text{INC1}}$$

and the solution to Eq. (2.15)^[GFEQ] will give the exact Green's function of the Pomeron. However, we prefer to develop a different technique for finding the Pomeron Green's function, which makes the calculation more transparent, and leads to explicit analytical formulas for physical observables (see section 3.1).

2.5 The phenomenological parameters and their typical values

Unfortunately, even with all assumptions that we have made, our approach is still phenomenological, since we have to determine the parameters of our interaction from a fit to the experimental data. However, using our main idea that the soft interaction stems from rather short distances, we are able to give some estimates for these parameters.

First, we list all of these parameters:

1. For description of Good-Walker mechanism of diffraction production in the two channel model, we need two phenomenological functions $g_1(b)$ and $g_2(b)$, which describe the vertices of interaction of the Pomeron with state 1 and 2 (see Eq. (2.2)^[2CHM31] and Eq. (2.2)^[2CHM31], and one number β see Eq. (2.2)^[2CHM31] and Eq. (2.2)^[2CHM31]);
2. The Pomeron intercept $\Delta = \alpha(0) - 1$;
3. The low energy amplitude of dipole -target interaction γ ;

Since we believe that the short distances contribute to the Pomeron structure we expect that

$$\Delta \propto \alpha_S; \quad \gamma \propto \alpha_S^2; \quad \tilde{g}_1 \approx \tilde{g}_2 \propto 1 \quad (2.18) \quad \boxed{\text{EST}}$$

For $\tilde{g}_i(b)$ we use the entire phenomenological assumption

$$\tilde{g}_i(b) = \tilde{g}_i S(b) = \frac{\tilde{g}_i}{4\pi} m_i^3 b K_1(m_i b) \quad (2.19) \quad \boxed{\text{S}}$$

where $S(b)$ is the Fourier transform of the dipole formula for the form factor $1/(1 + q^2/m_i^2)^2$.

3. Summing the enhanced diagram

In this section we sum the enhanced diagrams, and obtain the exact Green's function of the Pomeron, as well as the exact vertex for the triple Pomeron interaction. To achieve this we employ the approximation that has been developed in Ref. [53] (MPSI approximation), and the improved version as in Refs. [54, 55], so as to adjust this method for the summation of the Pomeron loop diagrams, for Pomerons with the intercept $\Delta > 0$.

3.1 Improved MPSI approximation

To illustrate the method, we calculate the first enhanced diagram of Fig. [Fig. 4](#) ^{[enh1](#)}

$$\begin{aligned} A(\text{Fig. 4})^{\text{enh1}} &= -g_1 g_2 G_{3P}^2 \int_0^Y dy_1 \int_0^{y_1} dy_2 G(Y - y_1) G^2(y_1 - y_2) G(y_2 - 0) \\ &= -g_1 g_2 G_{3P}^2 \int_0^Y dy_1 \int_0^{y_1} dy_2 e^{\Delta(Y + y_1 - y_2)} = -\frac{g_1 g_2 G_{3P}^2}{\Delta^2} \{e^{2\Delta Y} + e^{\Delta Y} + \Delta Y e^{\Delta Y}\} \\ &= \tilde{g}_1 \tilde{g}_2 \{\gamma^2 e^{2\Delta Y} + \gamma^2 e^{\Delta Y} + \Delta \gamma^2 Y e^{\Delta Y}\} \end{aligned} \quad (3.1)$$

where $G_{3P} = \Delta \gamma$ and $\tilde{g}_i = g_i/\sqrt{\gamma}$ (see Fig. [Fig. 5](#) ^{[enh1gf](#)} for the notation).

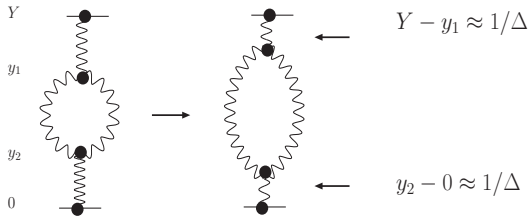


Figure 4: The first enhanced diagram for the Pomeron with intercept $\Delta > 0$. [enh1](#)

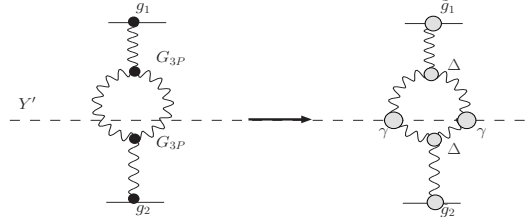


Figure 5: The first enhanced diagram in the form suited for the MPSI approximation. [enh1gf](#)

The main idea of the MPSI approximation is to take into account only the first term in Eq. [\(B.1\)](#) ^{[MPSI1](#)}, neglecting other terms, since they are suppressed as $\exp[-\Delta Y]$. This term is the result of integration for $Y - y_1 \approx 1/\Delta$ and $y_2 - 0 \approx 1/\Delta$ (see Fig. [Fig. 4](#) ^{[enh1](#)}). The general expression for the sum of the enhanced diagrams in MPSI approximation is shown in Fig. [Fig. 6](#) ^{[genmps1](#)}.

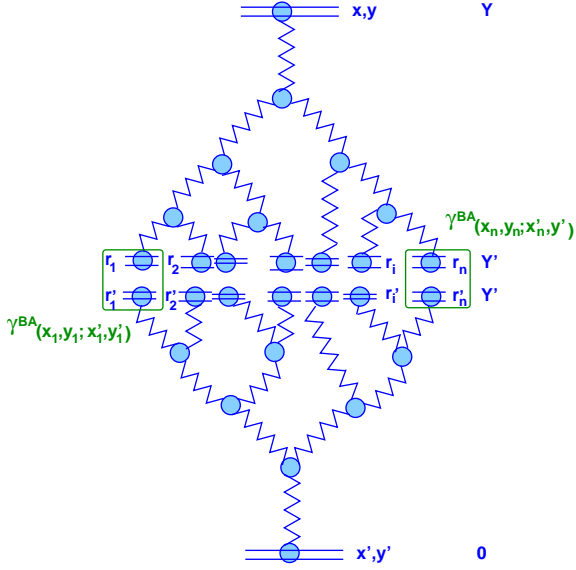


Figure 6: The exact Green's function of the Pomeron as a sum of enhanced diagrams in perturbative QCD in the MPSI approximation.

we will do it in a different way. First we introduce a new generating function

$$N(Y - Y', \gamma) \equiv 1 - Z(Y - Y', u = 1 - \gamma) \quad (3.2) \quad \boxed{\text{MPSI2}}$$

From Eq. (2.9) one can associate N with the scattering amplitude, when the variable γ is equal to the low energy parton amplitude. If we introduce a new variable

$$\gamma_R = \frac{\gamma}{1 - \gamma} \quad (3.3) \quad \boxed{\text{GR}}$$

Eq. (2.8) reduces to the form

$$\frac{\partial N(Y - Y'; \gamma_R)}{\partial (Y - Y')} = \Delta \gamma_R \frac{\partial N(Y - Y'; \gamma_R)}{\partial \gamma_R} \quad (3.4) \quad \boxed{\text{MPSI3}}$$

Eq. (3.4) is the equation for the system of non interacting Pomerons, and the general solution has the following form

$$N(Y - Y'; \gamma_R) = \sum_{n=1}^{\infty} (-1)^n C_n \gamma_R^n G^n(Y - 0) \quad (3.5) \quad \boxed{\text{MPSI4}}$$

where the coefficients C_n can be found from the initial conditions, namely, from the expression for the low energy amplitude. For summing the enhance diagrams the initial condition

$$N(Y - Y' = 0; \gamma_R) = \gamma = \gamma_R / (1 + \gamma_R) \quad (3.6) \quad \boxed{\text{MPSIIC}}$$

One can see that the MPSI approximation is the t -channel unitarity constraint adjusted to Reggeon Calculus, in the form of the generating functional (generating function in our case for summing Pomeron interactions). From this picture, and from our knowledge of the cascade described by the 'fan' diagrams, we can find the answer for the sum of enhanced diagrams only. The physical meaning of the introduced parameters is clear: γ is the low energy amplitude for two partons (dipoles) scattering at an arbitrary rapidity Y' , and Δ is the value of the vertex for the decay of one parton (dipole) to two parton (dipoles). It should be stressed that the answer does not depend on the value of Y' , but it should be chosen somewhere in the central region of the scattering.

To find the generating function that describes the sum of the 'fan' diagrams we need to solve Eq. (2.8).

This is not a difficult task, and for illustrative purposes

generates $C_n = 1$ and the solution is

$$N(Y - Y'; \gamma_R) = \frac{\gamma_R e^{\Delta(Y - Y')}}{1 + \gamma_R e^{\Delta(Y - Y')}} \quad (3.7) \quad \boxed{\text{MPSI5}}$$

The initial condition of Eq. (3.6) has very simple physics behind it, and has been discussed in Ref. [54].

The main idea of the improved MPSI approximation, is to replace γ_R in the generating function $N(\gamma_R|Y)$ by the low energy amplitude for the dipole-dipole interaction, (see Fig. 6). It is easy to see that the amplitude in the MPSI approximation has the form (in this equation we denote $N(\gamma_R|Y)$ by $N^{MFA}(\gamma_R|Y)$ where MFA stands for mean field approximation)

$$\begin{aligned} N^{MPSI}(Y) &= \\ &= \sum_{n=1}^{\infty} \frac{(-1)^n}{n!} \left(\frac{\partial}{\partial \gamma_R^{(1)}} \right)^n N^{MFA}(Y - Y'; \gamma_R^{(1)})|_{\gamma_R^{(1)}=0} \left(\frac{\partial}{\partial \gamma_R^{(2)}} \right)^n N^{MFA}(Y' - 0; \gamma_R^{(2)})|_{\gamma_R^{(2)}=0} \gamma_0^n \\ &= 1 - \exp \left\{ -\gamma_0 \frac{\partial}{\partial \gamma_R^{(1)}} \frac{\partial}{\partial \gamma_R^{(2)}} \right\} N^{MFA}(Y - Y'; \gamma_R^{(1)}) N^{MFA}(Y' - 0; \gamma_R^{(2)})|_{\gamma_R^{(1)}=\gamma_R^{(2)}=0} \end{aligned} \quad (3.8)$$

where γ_0 is the low energy amplitude for parton scattering (we will denote this amplitude as γ and hope that it will not cause any inconvenience).

3.2 The range of energy for which our approach is reliable

We return to the example of the first enhanced diagram (see Eq. (3.1)). The most dangerous term is the last one. It has an extra Y , which stems from the region of integration $y_1 - y_2 \approx 1/\Delta$, and it is the first term of the renormalization of the Pomeron intercept. One can see (see Refs. [54, 55] for details) that the renormalized intercept $\Delta_R = \Delta - \Delta\gamma^2$ *. This cannot be calculated in the MPSI approximation. Therefore, the first estimate for the range of energy where we can trust the MPSI approximation, comes from the demand that the renormalization of the Pomeron intercept should be small. This leads to

$$\Delta\gamma Y \ll 1; \quad \text{or} \quad Y \ll \frac{1}{\Delta\gamma} \quad (3.9) \quad \boxed{\text{ER1}}$$

However, a more restricted region can be obtained from Eq. (2.15). The term $-\gamma u^2 \partial^2 Z / \partial u^2$ describes the four Pomeron interaction, and as we have discussed, should be considered as small in our approach. Solving this equation without this term, and taking it into account as a perturbation, it is easy to show that the contribution of the four Pomeron interaction turns out to be small for

$$\gamma Y \ll 1; \quad \text{or} \quad Y \ll \frac{1}{\gamma} \quad (3.10) \quad \boxed{\text{ER2}}$$

*To understand, this it is sufficient to compare this term with the exchange of one Pomeron, which has the form $\tilde{g}_1 \tilde{g}_2 \gamma \exp(-\Delta Y)$ in our notation.

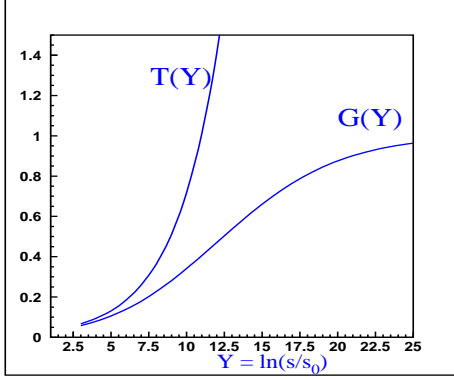


Figure 7: The exact Green's function of the Pomeron versus $Y = \ln(s/s_0)$ for $s_0 = 1 \text{ GeV}^2$, and $T(Y)$ for $\Delta = 0.339$ and $\gamma = 0.0242$. The values of parameters have been taken from our fit [7].

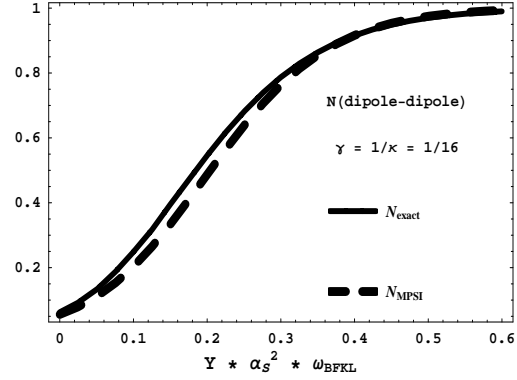


Figure 8: The comparison of the exact solution of Eq. (2.15) for the Pomeron Green's function $G(Y)$ (see Ref. [50,51]) with $G(Y)$ in the improved MPSI approximation (see Eq. (5.13)). The figure is taken from Ref. [51].

The second restriction of our approach, comes from the fact that we consider $\alpha'_{\mathcal{P}} = 0$. Inclusion of a small $\alpha'_{\mathcal{P}}$ will destroy our approximation for energies which we can find from the condition

$$\alpha'_{\mathcal{P}} Y > 1/m_i^2 \quad \text{or} \quad Y > \frac{1}{\alpha'_{\mathcal{P}} m_i^2} \quad (3.11) \quad \text{ER3}$$

Thus, we can trust the MPSI approximation in the region

$$Y \leq \min \left\{ \frac{1}{\gamma}, \frac{1}{\alpha'_{\mathcal{P}} m_i^2} \right\} \quad (3.12) \quad \text{ER4}$$

3.3 The Pomeron Green's function and the elastic scattering amplitude

Using Eq. (5.8) we can obtain the Green's function of the Pomeron in a closed form, namely [7]

$$G(Y) = 1 - \exp\left(-\frac{1}{T(Y)}\right) \frac{1}{T(Y)} \Gamma\left(0, \frac{1}{T(Y)}\right) \quad (3.13) \quad \text{ES1}$$

with

$$T(Y) = \gamma e^{\Delta Y} \quad (3.14) \quad \text{ES11}$$

and $\Gamma(0, 1/T)$ is the incomplete gamma function (see formulae 8.35 in Ref. [58]). Using this function we can write the opacities in the two channel formalism (see Eq. (2.5)) in the form

$$\Omega_{i,k} = \tilde{g}_i(b) \tilde{g}_k(b) G(Y) \quad (3.15) \quad \text{ES2}$$

It should be stressed that the Green's function of Eq. (5.13) has been found for high energies, where the MPSI approach is correct. However, the theory given by the functional of Eq. (2.11) has an analytical

solution (see Refs. [50, 51]) at arbitrary values of the energy. Comparison with the improved MPSI approximation (see Fig. [5](#) ^{compar}) shows that this approximation describes the lowest energy within accuracy of 5 to 10 %, for $\gamma = 1/16$. In our fit [7] $\gamma = 0.0242$ which leads to even better accuracy. Therefore, we can safely use the improved MPSI approximation starting from $s = 400 \text{ GeV}^2$ which was used in our fit.

The elastic amplitude is equal

$$a_{el}(b) = i (\alpha^4 A_{1,1} + 2\alpha^2 \beta^2 A_{1,2} + \beta^4 A_{2,2}) \quad (3.16) \quad \text{ES3}$$

where $A_{i,k}$ is given by Eq. [\(2.5\)](#) ^{2CHM1} with $\Omega_{i,k}$ from Eq. [\(3.15\)](#) ^{ES2}.

The Pomeron Green's function tends to unity at large values of the argument T . In Fig. [7](#) ^{pomgrf} we plot this function as well as $T(Y)$ for $\Delta = 0.339$ and $\gamma = 0.0242$ these values were found in our fit (see Ref. [7] and below). One can see that $G(Y)$ is quite different from the one Pomeron exchange, even in the region when T is smaller than 1.

In the MPSI approximation, the exact triple Pomeron vertex (see Fig. [2](#) ^{enhst}) is equal to the 'bare' vertex.

One more comment should be made: Eq. [\(3.13\)](#) ^{ES1} leads to

$$G(Y) = \sum_{n=1}^{\infty} (-1)^{n+1} n! T^n(Y) \quad (3.17) \quad \text{ES4}$$

which is a typical Borel summable asymptotical series. Such an amplitude cannot be obtained as a solution of the equation after a finite number of integrations.

3.4 The exact vertex and diffractive production

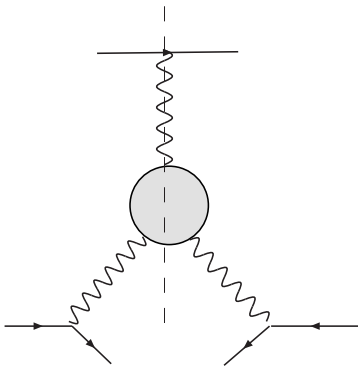


Figure 9: The first diagram for single diffraction. The wavy lines and the blob denote the exact [sd2](#) Green's function and exact vertex for Pomerons [7].

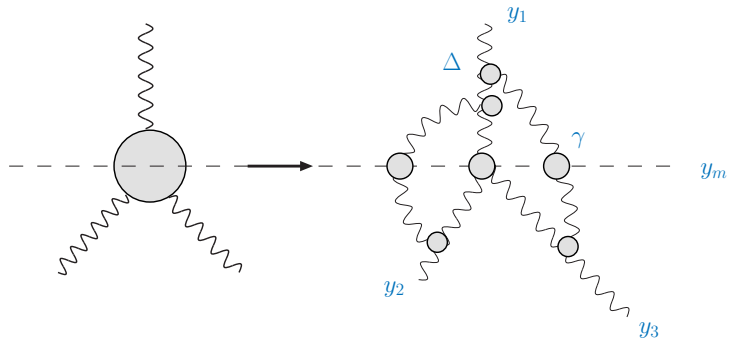


Figure 10: The diagrams that contribute to the exact vertex.

[sd1](#)

The process of single diffraction has not been taken into account in the Green's function of the Pomeron. In our paper of Ref. [7] we calculated the first diagram for the single diffraction dissociation, namely one

in Fig. ^{sd1}9. In this diagram both the Pomeron Green's function, and the vertex are exact. We found that this contribution leads to a small cross section for single diffraction in the region of the large mass, and we view this calculation as just the first attempt to solve the problem of the summation of all diagrams. We will solve this problem in the next section. The cross section for single diffraction has been calculated in Ref. [7] using the MPSI approximation. Here, we calculate the exact vertex shown in Fig. ^{sd2}10. We can use Eq.3.34 of Ref. [7], where we only need to extract the contribution from the external Green's function of the Pomeron, and introduce three rapidities as shown in Fig. ^{sd2}10. The final equation has the form

$$\Gamma^{MPSI}(y_1, y_2, y_3) = \quad (3.18)$$

$$\begin{aligned} & \sum_{n=1; m=1}^{\infty} \frac{(-1)^{n+m}}{n! m!} \gamma^{n+m} \frac{\partial^n}{\partial^n w^p} \frac{\partial^m}{\partial^n \bar{w}^p} \Gamma_{sd}^{MFA}(w^p, \bar{w}^p; y_1 - y_m) |_{w=1; \bar{w}=1} \\ & \times \frac{\partial^n \Gamma^{MFA}(w^t, y_m - y_2) |_{w^t=1}}{\partial^n w^t} \frac{\partial^m \Gamma^{MFA}(\bar{w}^t, y_m - y_3) |_{\bar{w}^t=1}}{\partial^n \bar{w}^t} \\ & = \frac{\Delta}{4} \frac{1}{T(y_1 - y_2) - T(y_1 - y_3)} \{ \Gamma_1(2T(y_1 - y_2)) - \Gamma_1(2T(y_1 - y_3)) \} \end{aligned} \quad (3.19)$$

$$\text{with } \Gamma_1(T) = (1/T^3) \times \{ T(1+T) - \exp(-1/T) (1+2T) \Gamma(0, 1/T) \} \quad (3.20)$$

where

$$\Gamma^{MFA}(w, \bar{w}; y_1 - y_m) = 2 \Delta w \bar{w} \frac{1}{(1 + (w + \bar{w})(e^{\Delta(y_1 - y_m)} - 1))^2} \quad (3.21) \quad \boxed{\text{SD41}}$$

and

$$\Gamma^{MFA}(w; y_m - y_i) = \frac{1}{(1 + w(e^{\Delta(y_m - y_i)} - 1))} \quad (3.22) \quad \boxed{\text{SD42}}$$

where w and \bar{w} are the variables that we needed to introduce, as has been explained in Ref. [7]. It is easy to see that

$$\Gamma^{MPSI}(y_1, y_2, y_3) \xrightarrow{y_1 - y_2 \gg 1; y_1 - y_3 \gg 1} \frac{\Delta}{8} e^{-\Delta(2y_1 - y_2 - y_3)} \quad (3.23) \quad \boxed{\text{SD5}}$$

and therefore, to a good accuracy we can consider that the exact vertex is equal to the bare one, namely, $\Gamma^{MPSI}(y_1, y_2, y_3) = \Delta$.

The double diffraction contained in the Pomeron Green's function has been calculated directly using the unitarity constraint (see Ref. [7]).

4. Summing the full set of diagrams

4.1 Elastic scattering

In this section we sum the full set of the diagrams using the improved MPSI approximation. In our approach that has been discussed in the previous section, the elastic amplitude is written as the sum of the eikonal diagrams for each state i in the two channel model, with the exact Pomeron Green's function (see Fig. ^{fulset}11-A). Here we sum all diagrams (see Fig. ^{fulset}11-B) using the MPSI approximation. The diagrams of

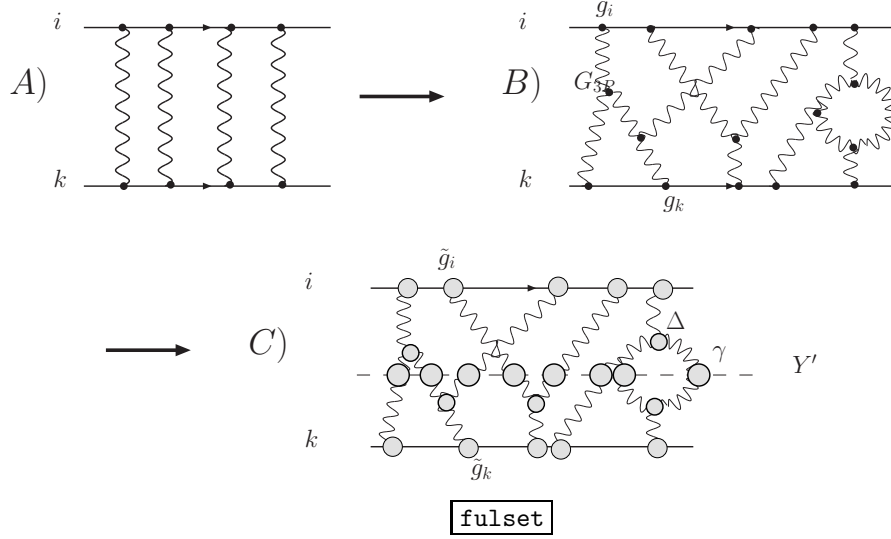


Figure 11: The full set of the diagrams. Fig. [II-A](#) the sum of enhanced diagrams in the two channel approach, Fig. [II-B](#) shows the full set of the diagrams which in Fig. [II-C](#) is pictured in a way that is most suitable to illustrate the MPSI approach. The bold wavy line stands for the exact Pomeron Green's function that includes all enhanced diagrams.

Fig. [II-B](#) (in the MPSI approximation), are shown in Fig. [II-C](#). The first step in determining this sum is to find the solution to Eq. [\(3.4\)](#) with the initial condition

$$N_{in}(\gamma; Y - Y' = 0) = 1 - e^{-\tilde{g}_i \gamma} \quad (4.1) \quad \text{FSE1}$$

The meaning of this conditions is very simple and stems from Eq. [\(2.9\)](#): Eq. [\(4.1\)](#) gives the eikonal formula for the scattering amplitude for $Y - Y' = 0$. The general solution of Eq. [\(3.4\)](#) is simple, namely,

$$N^{MFA}(Y - Y'; \gamma_R) = N_{in}(\gamma = N(Y - Y'; \gamma_R)) \quad (4.2) \quad \text{FSE2}$$

where $N(Y - Y'; \gamma_R)$ is given by Eq. [\(3.5\)](#).

For the initial condition of Eq. [\(4.1\)](#)

$$N^{MFA}(Y - Y'; \gamma_R) = 1 - \exp \left\{ -\tilde{g}_i \frac{\gamma_R e^{\Delta(Y-Y')}}{1 + \gamma_R e^{\Delta(Y-Y')}} \right\} \quad (4.3) \quad \text{FSE3}$$

Using the generating function for Laguerre polynomials (see Ref. [58] formula **8.973(1)**), namely

$$(1 - z)^{-\alpha-1} \exp \left(\frac{xz}{z-1} \right) = \sum_{n=0}^{\infty} L_n^\alpha(x) z^n \quad (4.4) \quad \text{LPGF}$$

we obtain for Eq. [\(4.3\)](#)

$$N^{MFA}(Y - Y'; \gamma_R) = - \sum_{n=1}^{\infty} L_n^{-1}(\tilde{g}_i) \left(-\gamma_R e^{\Delta(Y-Y')} \right)^n \quad (4.5) \quad \boxed{\text{FSE4}}$$

Using Eq. (4.5) and Eq. (3.8) we have for the scattering amplitude

$$N^{MFA}(Y;) = \sum_{n=0}^{\infty} n! L_n^{-1}(\tilde{g}_i) L_n^{-1}(\tilde{g}_k) (-\gamma e^{\Delta Y})^n \quad (4.6) \quad \boxed{\text{FSE5}}$$

Introducing $n! = \int_0^{\infty} \xi^n e^{-\xi} d\xi$ we can re-write Eq. (4.6) in the form

$$N^{MFA}(Y;) = \int_0^{\infty} d\xi e^{-\xi} d \sum_{n=0}^{\infty} L_n^{-1}(\tilde{g}_i) L_n^{-1}(\tilde{g}_k) (-\xi \gamma_0 e^{\Delta Y})^n \quad (4.7) \quad \boxed{\text{FSE6}}$$

Using formula 8.976(1) of Ref. [58], namely

$$\sum_{n=0}^{\infty} n! z^n \frac{L_n^{\alpha}(x) L_n^{\alpha}(y)}{\Gamma(n + \alpha + 1)} = \frac{(x y z)^{-\frac{1}{2}\alpha}}{1 - z} \exp\left(-z \frac{x + y}{1 - z}\right) I_{\alpha}\left(2 \frac{\sqrt{x y z}}{1 - z}\right) \quad (4.8) \quad \boxed{\text{SUML}}$$

we derive the final result

$$N_{i,k}^{MFA}(Y) = \int_0^{\infty} \frac{d\xi}{\xi} e^{-\xi} \frac{(\tilde{g}_i \tilde{g}_k \xi T(Y))^{\frac{1}{2}}}{1 + \xi T(Y)} \exp\left\{-\xi T(Y) \frac{\tilde{g}_i + \tilde{g}_k}{1 + \xi T(Y)}\right\} J_1\left(2 \frac{\sqrt{\tilde{g}_i \tilde{g}_k \xi T(Y)}}{1 + \xi T(Y)}\right) \quad (4.9) \quad \boxed{\text{FSE7}}$$

where

$$T(Y) = \gamma e^{\Delta Y} \text{ where } \gamma \equiv \gamma_0. \quad (4.10) \quad \boxed{\text{T}}$$

Eq. (4.9) reduces to a simple and elegant formula in the case that we can consider $\tilde{g}_i T(Y) \sim 1$, $\tilde{g}_i \tilde{g}_k T(Y) > 1$ but $T(Y) \ll 1$. Indeed, in this case the integral over ξ can be taken and

$$A_{i,k}(Y; b) = 1 - \exp\left\{-\frac{1}{2} \frac{\tilde{g}_i \tilde{g}_k T(Y)}{1 + T(Y) [\tilde{g}_i + \tilde{g}_k]}\right\} \quad (4.11) \quad \boxed{\text{FSE9}}$$

In Eq. (4.9) we neglected b dependence. In our approach, the b dependence enters through the vertices $\tilde{g}_i(b)$. For Eq. (4.11) it is easy to write the expression that takes into account the correct impact parameter behaviour, namely, it has the form

$$A_{i,k}(Y; b) = 1 - \exp\left\{-\frac{1}{2} \int d^2 b' \frac{\left(\tilde{g}_i(\vec{b}') \tilde{g}_k(\vec{b} - \vec{b}') T(Y)\right)}{1 + T(Y) [\tilde{g}_i(\vec{b}') + \tilde{g}_k(\vec{b} - \vec{b}')]}\right\} \quad (4.12) \quad \boxed{\text{FSE91}}$$

To obtain the elastic amplitude we need to substitute the amplitudes $A_{i,k}$ in Eq. (3.16).

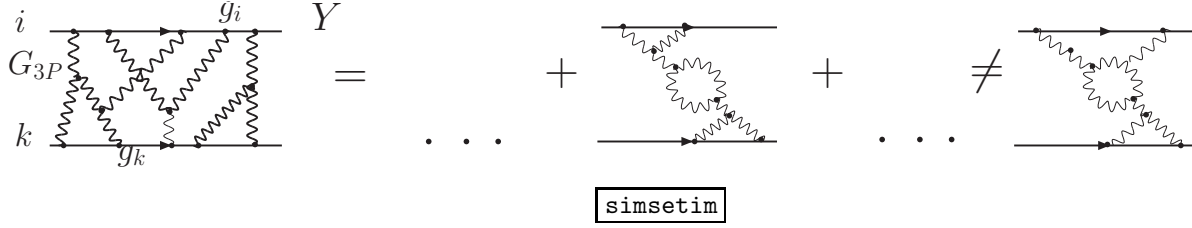


Figure 13: The set of diagrams that is selected and summed using the fact that $\tilde{g}_i G(T(Y)) \geq 1$ while $\Delta^2 G(T(Y)) \ll 1$.

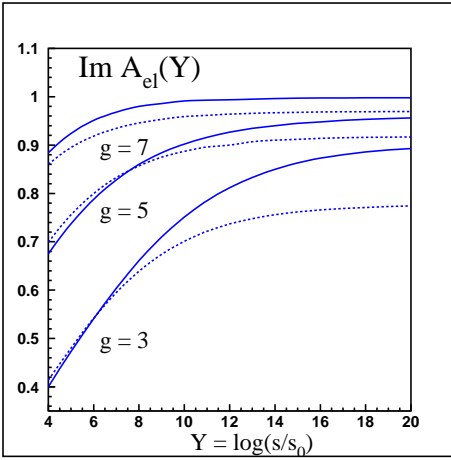


Figure 12: Comparison of the exact imaginary part of the elastic amplitude, given by Eq. (4.9), with the approximation for $\tilde{g}T(Y) \approx 1$ while $\Delta T(Y) \ll 1$. The values of $\gamma = 0.0242$ and $\Delta = 0.339$ were taken from the fit [7] using the sum of enhanced diagrams (see section 3)

For the nucleus-nucleus scattering Eq. (4.11) is the generalization of the Glauber formula, and we intend publishing our estimates for the cross section of nucleus-nucleus scattering elsewhere.

Eq. (4.11) is very simple and we intend to use this approximation for the description of the experimental data. We plot in Fig. 12 the comparison of $Im A_{el}(Y)$ given by the correct Eq. (4.9), with the approximate Eq. (4.11) for $\gamma = 0.0242$ and $\Delta = 0.339$ at the values of $\tilde{g}_1 = \tilde{g}_2 = 3$ and 5. The values of parameters γ and Δ are taken from our fit [7] with the amplitude that takes into account the enhanced diagrams only (see section 3). Note that at large \tilde{g} , the accuracy of the approximate solution is about 5%, while at low values of \tilde{g} the errors could be as large as 12%. (see Fig. 12).

Eq. (4.12) can be derived by direct summation of the Pomeron diagrams, without assuming the MPSI approximation (see Ref. [8]).

Using the fact that Eq. (4.12) sums the net set of the diagrams not only in the MPSI approximation, we can also sum more complicated diagrams in which the 'bare' Pomerons in Fig. 11-C are replaced by the exact Pomeron of Eq. (5.13) (see Fig. 13, where we show examples of the diagrams that we sum, as well as examples of the diagrams that we still need to calculate. In the selection of these diagrams we used parameters: $\tilde{g}_{i,k} G(T(Y)) \geq 1$ and $\Delta^2 G(T(Y)) \ll 1$. In the fit of Ref. [7] $\tilde{g} \geq 5.8$ and $\Delta = 0.339$ and, therefore, we can obtain the scattering amplitude using this re-summation procedure within the accuracy $\Delta^2/\tilde{g}_i \leq 0.1/5.8 = 0.02$. We need only to replace $T(Y)$ in Eq. (4.12) by $G(T(Y))$.

4.2 Diffractive production

To calculate the single diffraction process it is necessary to introduce three different variables : $\gamma_R, \bar{\gamma}_R$ and γ_{in} to describe Pomerons in the amplitude, in the complex conjugate amplitude, and the amplitude of

the cut Pomeron, respectively (see Ref. [54] for details). The difference to the calculation of the elastic amplitude lies mostly in the fact that we need to take into account all three amplitudes in Eq. (5.8). For the case of single diffraction, we have only one cut Pomeron at $Y = Y_m$ that decays in one γ_R Pomeron, and one $\bar{\gamma}_R$ Pomeron. Therefore, the cut Pomeron in Fig. 14 has the following form [54]

$$N_{\text{cut Pomeron}}^{MFA}(\gamma_R, \bar{\gamma}_R; Y - Y_M \equiv Y_m = \ln(M^2/s_0)) = 2 \Delta_P \gamma_R \bar{\gamma}_R \frac{e^{\Delta_P Y_m}}{(1 + (\gamma_R + \bar{\gamma}_R) e^{\Delta_P Y_m})^2} \quad (4.13) \quad \boxed{\text{FSSD1}}$$

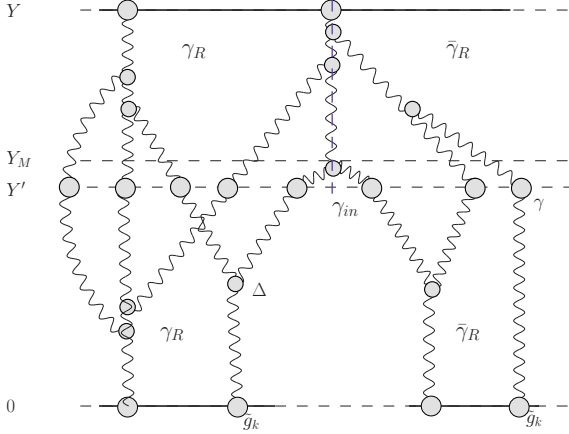


Figure 14: The MPSI approximation for the cross section for single diffractive production of mass ($M^2, Y - Y_M = \ln(M^2/s_0)$). The dashed lines show the cut Pomerons. All other notations, are as in Fig. 11. $\boxed{\text{sdst}}$

Choosing $Y' = Y_M$ we have the $N^{MFA}(\gamma_R, \bar{\gamma}_R; Y - Y_M \equiv Y_m = \ln(M^2/s_0))$ for the full set of the diagrams in the form

$$N^{MFA}(\gamma_R, \bar{\gamma}_R; Y - Y_M = \ln(M^2/s_0) \equiv Y_m) = \quad (4.14)$$

$$N_{\text{cut Pomeron}}^{MFA}(\gamma_R, \bar{\gamma}_R; Y - Y_M = \ln(M^2/s_0) \equiv Y_m) \exp\left(-\frac{\tilde{g}_i \gamma_R e^{\Delta Y_m}}{1 + \gamma_R e^{\Delta Y_m}}\right) \exp\left(-\frac{\tilde{g}_i \bar{\gamma}_R e^{\Delta Y_m}}{1 + \bar{\gamma}_R e^{\Delta Y_m}}\right)$$

Using Eq. (4.13) we can reduce Eq. (4.14) to the form

$$N^{MFA}(\gamma_R, \bar{\gamma}_R; Y - Y_M = \ln(M^2/s_0) \equiv Y_m) = \quad (4.15)$$

$$2 \Delta_P \gamma_R \bar{\gamma}_R \int t dt e^{-t(1+(\gamma_R+\bar{\gamma}_R)\exp(\Delta Y_m))} \exp\left(-\frac{\tilde{g}_i \gamma_R e^{\Delta Y_m}}{1 + \gamma_R e^{\Delta Y_m}}\right) \exp\left(-\frac{\tilde{g}_i \bar{\gamma}_R e^{\Delta Y_m}}{1 + \bar{\gamma}_R e^{\Delta Y_m}}\right)$$

Using Eq. (4.4) and Eq. (4.5) we can expand N^{MFA} with respect to powers of $\gamma_R \exp(\Delta Y_m)$ and $\bar{\gamma}_R \exp(\Delta Y_m)$, namely

$$N^{MFA}(\gamma_R, \bar{\gamma}_R; Y - Y_M = \ln(M^2/s_0) \equiv Y_m) = \quad (4.16)$$

$$2 \Delta \tilde{g}_i e^{-\Delta Y_m} \sum_{N=n+\bar{n}} \sum_{k=0}^n \sum_{\bar{k}=0}^{\bar{n}} \frac{t^{k+\bar{k}}}{k! \bar{k}!} (-1)^N \gamma^n \bar{\gamma}^{\bar{n}} (-e^{\Delta Y_m})^N L_{n-k-1}^{-1}(-\tilde{g}_i) L_{\bar{n}-\bar{k}-1}^{-1}(-\tilde{g}_i)$$

where n, k, \bar{n} and \bar{k} are integer numbers.

Using formulae **8.972(1)** and **9.211(2)** of Ref. [58] we obtain

$$L_n^\alpha(-g) = \frac{1}{n!} e^{-g} (-g)^{-\frac{\alpha}{2}} \int_0^\infty d\xi e^{-\xi} \xi^{n+\frac{\alpha}{2}} J_\alpha \left(2\sqrt{g\xi} \right) \quad (4.17) \quad \boxed{\text{FSSD5}}$$

Substituting Eq. $\boxed{\text{FSSD5}}$ in Eq. $\boxed{\text{FSSD4}}$ we have

$$\begin{aligned} N^{MFA}(\gamma_R, \bar{\gamma}_R; Y_m) &= 2 \Delta \tilde{g}_i e^{-\Delta Y_m} \sum_{N=n+\bar{n}} \sum_{k=0}^n \sum_{\bar{k}=0}^{\bar{n}} \frac{t^{k+\bar{k}}}{k! \bar{k}!} (-1)^N \gamma^n \bar{\gamma}^{\bar{n}} (-e^{\Delta Y_m})^N \\ &\times \frac{1}{(n-k-1)!} e^{-\tilde{g}_i} (-\tilde{g}_i)^{\frac{1}{2}} \int_0^\infty d\xi e^{-\xi} \xi^{n+\frac{\alpha}{2}} J_1 \left(2\sqrt{\tilde{g}_i \xi} \right) \\ &\times \frac{1}{(\bar{n}-\bar{k}-1)!} e^{-\tilde{g}_i} (-\tilde{g}_i)^{\frac{1}{2}} \int_0^\infty d\bar{\xi} e^{-\bar{\xi}} \bar{\xi}^{\bar{n}+\frac{\alpha}{2}} J_1 \left(2\sqrt{\tilde{g}_i \bar{\xi}} \right) \end{aligned} \quad (4.18)$$

The generating function that describes the low cascade is equal to

$$N^{MFA}(\gamma_R, \bar{\gamma}_R; Y - Y_m) = N^{MFA}(\gamma_R; Y - Y_m | Eq. \boxed{\text{FSE4}}) \times N^{MFA}(\bar{\gamma}_R; Y - Y_m | Eq. \boxed{\text{FSE4}}) \quad (4.19) \quad \boxed{\text{FSSD7}}$$

and can be re-written in the following form

$$\begin{aligned} N^{MFA}(\gamma_R, \bar{\gamma}_R; Y - Y_m) &= \sum_{N=n+\bar{n}} \sum_{k=0}^n (-1)^N \gamma^n \bar{\gamma}^{\bar{n}} \left(-e^{\Delta(Y-Y_m)} \right)^N \\ &\times \frac{1}{n!} e^{-\tilde{g}_k} (-\tilde{g}_k)^{\frac{1}{2}} \int_0^\infty d\xi e^{-\xi} \xi^{n+\frac{\alpha}{2}} J_1 \left(2\sqrt{\tilde{g}_k \xi} \right) \\ &\times \frac{1}{\bar{n}!} e^{-\tilde{g}_k} (-\tilde{g}_k)^{\frac{1}{2}} \int_0^\infty d\bar{\xi} e^{-\bar{\xi}} \bar{\xi}^{\bar{n}+\frac{\alpha}{2}} J_1 \left(2\sqrt{\tilde{g}_k \bar{\xi}} \right) \end{aligned} \quad (4.20)$$

Eq. $\boxed{\text{MPSI6}}$ should be replaced by a more general equation, namely,

$$\begin{aligned} N_{SD}^{MPSI}(Y_m; Y - Y_m) &= \sum_{n=1}^\infty \frac{(-1)^n}{n!} \sum_{\bar{n}=1}^\infty \frac{(-1)^{\bar{n}}}{\bar{n}!} (\gamma_0 T_{SD})^{n+\bar{n}} \\ &\times \left(\frac{\partial}{\partial \gamma_R^{(1)}} \right)^n \left(\frac{\partial}{\partial \bar{\gamma}_R^{(1)}} \right)^{\bar{n}} N^{MFA} \left(Y_m; \gamma_R^{(1)}, \bar{\gamma}_R^{(1)} \right) \Big|_{\gamma_R^{(1)}=\bar{\gamma}_R^{(1)}=0} \\ &\times \left(\frac{\partial}{\partial \gamma_R^{(2)}} \right)^n \left(\frac{\partial}{\partial \bar{\gamma}_R^{(2)}} \right)^{\bar{n}} N^{MFA} \left(Y - Y_m; \gamma_R^{(2)}, \bar{\gamma}_R^{(2)} \right) \Big|_{\gamma_R^{(2)}=\bar{\gamma}_R^{(2)}=0} \end{aligned} \quad (4.21)$$

Using Eq. $\boxed{\text{FSSD5}}$ we can sum over k and \bar{k} reducing Eq. $\boxed{\text{FSSD6}}$ to the following equation

$$\begin{aligned} N^{MFA} \left(\gamma_R^{(1)}, \bar{\gamma}_R^{(1)}; Y_m \right) &= 2 \Delta \gamma_R^{(1)} \bar{\gamma}_R^{(1)} e^{-\Delta Y_m} T_{SD}^2 \tilde{g}_i e^{-2\tilde{g}_i} \sum_{n=1}^\infty \frac{(-1)^n}{(n-1)!} \sum_{\bar{n}=1}^\infty \frac{(-1)^{\bar{n}}}{(\bar{n}-1)!} \\ &\times \int t dt \int d\xi_1 (\xi_1 + t)^{n-1} \int d\bar{\xi}_1 (\bar{\xi}_1 + t)^{\bar{n}-1} (\xi_1 \bar{\xi}_1)^{-\frac{1}{2}} e^{-\xi_1 - \bar{\xi}_1} J_1 \left(2\sqrt{\tilde{g}_i \xi_1} \right) J_1 \left(2\sqrt{\tilde{g}_i \bar{\xi}_1} \right) \end{aligned} \quad (4.22)$$

Using Eq. (4.22) we can reduce Eq. (4.21) to the form

$$N_{SD}^{MPSI}(Y_m; Y - Y_m) = 2\Delta \tilde{g}_i \gamma_0^2 e^{-\Delta Y_m} T_{SD}^2(Y, Y_m) \int t dt e^{-t-\tilde{g}_i-\tilde{g}_k} \int d\xi_1 d\xi_2 e^{-\xi_1-\xi_2} \frac{\xi_2}{\sqrt{\xi_1 \xi_2}} \quad (4.23)$$

$$\times \sum_{n=1}^{\infty} \frac{1}{(n-1)!} (t + \xi_1)^{n-1} \xi_2^{n-1} J_1\left(2\sqrt{\tilde{g}_i \xi_1}\right) J_1\left(2\sqrt{\tilde{g}_k \xi_2}\right) \times \{\xi_1 \rightarrow \bar{\xi}_1; \xi_2 \rightarrow \bar{\xi}_2; n \rightarrow \bar{n}\} \times (-\gamma_0 T_{SD})^{n+\bar{n}}$$

Summing over n and \bar{n} we obtain

$$N_{SD}^{MPSI}(Y_m; Y - Y_m) = \quad (4.24)$$

$$2\Delta e^{-\Delta Y_m} T_{SD}^2(Y, Y_m) \tilde{g}_k^{-1} e^{-2\tilde{g}_i-2\tilde{g}_k} \int t dt \int d\xi_1 d\xi_2 d\bar{\xi}_1 d\bar{\xi}_2 e^{-t(\xi_2+\bar{\xi}_2)\gamma T_{SD}-t} e^{-\xi_1-\xi_2-\bar{\xi}_1-\bar{\xi}_2}$$

$$\times \frac{\xi_2 \bar{\xi}_2}{\sqrt{\xi_1 \xi_2}} \frac{1}{\sqrt{\bar{\xi}_1 \bar{\xi}_2}} e^{-\gamma \xi_1 \xi_2 T_{SD}} e^{-\gamma \bar{\xi}_1 \bar{\xi}_2 T_{SD}} J_1\left(2\sqrt{\tilde{g}_i \xi_1}\right) J_1\left(2\sqrt{\tilde{g}_i \bar{\xi}_1}\right) J_1\left(2\sqrt{\tilde{g}_k \xi_2}\right) J_1\left(2\sqrt{\tilde{g}_k \bar{\xi}_2}\right)$$

and after iteration over t we have

$$N_{SD}^{MPSI}(Y_m; Y - Y_m) = \quad (4.25)$$

$$2\Delta e^{-\Delta Y_m} T_{SD}^2(Y, Y_m) \tilde{g}_k^{-1} e^{-2\tilde{g}_i+2\tilde{g}_k} \int \frac{d\xi_1 d\xi_2 d\bar{\xi}_1 d\bar{\xi}_2}{(1 + (\xi_2 + \bar{\xi}_2) \gamma T_{SD})^2} e^{-\xi_1-\xi_2-\bar{\xi}_1-\bar{\xi}_2} \quad (4.26)$$

$$\times \frac{\xi_2 \bar{\xi}_2}{\sqrt{\xi_1 \xi_2}} \frac{1}{\sqrt{\bar{\xi}_1 \bar{\xi}_2}} e^{-\gamma \xi_1 \xi_2 T_{SD}} e^{-\gamma \bar{\xi}_1 \bar{\xi}_2 T_{SD}} J_1\left(2\sqrt{\tilde{g}_i \xi_1}\right) J_1\left(2\sqrt{\tilde{g}_i \bar{\xi}_1}\right) J_1\left(2\sqrt{\tilde{g}_k \xi_2}\right) J_1\left(2\sqrt{\tilde{g}_k \bar{\xi}_2}\right)$$

Introducing new variables $y = \xi_1 \xi_2$ and $\bar{y} = \bar{\xi}_1 \bar{\xi}_2$ and integrating over them, we obtain the final formula for the single diffraction amplitude $A_{i,k}(Y, Y_m)$ in the form

$$A_{i,k,l}^{SD}(Y, Y_m) = 2\Delta e^{-\Delta Y_m} T_{SD}^2(Y, Y_m) \tilde{g}_i \sqrt{\tilde{g}_k \tilde{g}_l} e^{-2\tilde{g}_i-\tilde{g}_k-\tilde{g}_l} \int \frac{d\xi_2 d\bar{\xi}_2 \sqrt{\xi_2 \bar{\xi}_2}}{(1 + (\xi_2 + \bar{\xi}_2) \gamma T_{SD})^2} e^{-\xi_2-\bar{\xi}_2} \quad (4.27)$$

$$\times J_1\left(2\sqrt{\tilde{g}_k \xi_2}\right) J_1\left(2\sqrt{\tilde{g}_l \bar{\xi}_2}\right) \left\{1 - \exp\left(\frac{-\tilde{g}_i}{1 + \xi_2 T_{SD}}\right)\right\} \left\{1 - \exp\left(\frac{-\tilde{g}_i}{1 + \bar{\xi}_2 T_{SD}}\right)\right\}$$

where

$$T_{SD}(Y; Y_m) = \gamma (e^{\Delta Y_m} - 1) e^{\Delta(Y-Y_m)} \quad (4.28) \quad \boxed{\text{TSD}}$$

In Eq. (4.27) we took into account that in the two channel model, the low cascade could be initiated by different states (k and l). As in the case of the elastic amplitude, \tilde{g}_i in Eq. (4.27) should be replaced by $\tilde{g}_i(\vec{b}')$ and by $\tilde{g}_{k,l}(\vec{b} - \vec{b}')$ and should be integrated over $d^2 b'$.

The total cross section of the diffractive production can be written as a sum of two terms: the Good-Walker term which is equal to

$$\sigma_{SD}^{GW} = \int d^2 b \left(\alpha \beta \{-\alpha^2 A_{1,1}^{el} + (\alpha^2 - \beta^2) A_{1,2}^{el} + \beta^2 A_{2,2}^{el}\} \right)^2 \quad (4.29) \quad \boxed{\text{FSSDGW}}$$

where $A_{i,k}$ are given by Eq. (FSE9), and the term which describes the diffractive production in the region of large mass, namely

$$\begin{aligned} \sigma_{SD}^{\text{Large mass}} = & 2 \int dY_m \int d^2b \\ & \left\{ \alpha^6 A_{1;1,1}^{SD} e^{-\Omega_{11}(Y;b)} + \alpha^2 \beta^4 A_{1;2,2}^{SD} e^{-\Omega_{12}(Y;b)} + 2 \alpha^4 \beta^2 A_{1;1,2}^{SD} e^{-\frac{1}{2}(\Omega_{11}(Y;b) + \Omega_{12}(Y;b))} \right. \\ & \left. + \beta^2 \alpha^4 A_{2;1,1}^{SD} e^{-\Omega_{12}(Y;b)} + 2 \beta^4 \alpha^2 A_{2;1,2}^{SD} e^{-\frac{1}{2}(\Omega_{12}(Y;b) + \Omega_{22}(Y;b))} + \beta^6 A_{2;2,2}^{SD} e^{-\Omega_{22}(Y;b)} \right\} \end{aligned} \quad (4.30)$$

To find the cross section for double diffraction we use the s -channel unitarity constraints as was suggested in Ref. [7]

$$2A_{i,k}^{el}(Y;b) = |A_{i,k}^{el}(Y;b)|^2 + 2A_{i,k,k}^{SD}(Y;b) + A_{i,k}^{DD} + A_{i,k}^{in}(Y;b) \quad (4.31) \quad \boxed{\text{FSDD1}}$$

It has been shown in Refs. [47, 54, 59] that the inelastic amplitude $A_{i,k}^{in}(Y;b) = A_{i,k}^{el}(2T(Y);b)$. Therefore, from Eq. (FSDD1) the amplitude for double diffraction production is equal to

$$\begin{aligned} A_{i,k}^{DD}(Y;b) = & \\ 2A_{i,k}^{el}(T(Y);b) - |A_{i,k}^{el}(T(Y);b)|^2 - 2 \int dY_m A_{i,k,k}^{SD}(T_{SD}(Y, Y_m; b); b) - A_{i,k}^{el}(2T(Y);b) \end{aligned} \quad (4.32)$$

Finally, the cross section of the double diffractive production is the sum of the Good-Walker contribution, which has the form

$$\sigma_{DD}^{GW} = \int d^2b \alpha^2 \beta^2 \left\{ A_{1,1}^{el} - 2A_{1,2}^{el} + A_{2,2}^{el} \right\}^2 \quad (4.33) \quad \boxed{\text{FSDD3}}$$

with $A_{i,k}^{el}$ given by Eq. (FSE9), and the term which is determined by the Pomeron interaction, and which contributes to the production of large masses. namely,

$$\sigma_{DD}^{\text{Large mass}} = \int d^2b \left\{ \alpha^4 A_{1,1}^{DD} e^{-\Omega_{11}(Y;b)} + 2\alpha^2 \beta^2 A_{1,2}^{DD} e^{-\Omega_{12}(Y;b)} + \beta^4 A_{2,2}^{DD} e^{-\Omega_{22}(Y;b)} \right\} \quad (4.34) \quad \boxed{\text{FSDD4}}$$

5. Corrections to our approach

5.1 $\alpha'_{\mathcal{P}} \neq 0$ and the Pomeron as a fixed branch point

In constructing our model we have made two assumptions that considerably simplify our approach. Firstly, we considered the case of $\alpha'_{\mathcal{P}} = 0$ for summation of the enhanced diagrams, in spite of the fact that $\alpha'_{\mathcal{P}} \approx 0.02 \text{ GeV}^{-2}$, is the value obtained from our fit of the experimental data. Secondly, we replaced the Pomeron Regge pole by a fixed square root singularity, that appears in the N=4 SYM. Both these assumptions are not principle in nature, but have been made to facilitate the simplicity and transparency of our approach. In this section we will expand our formalism so as to assess the consequence of our assumptions.

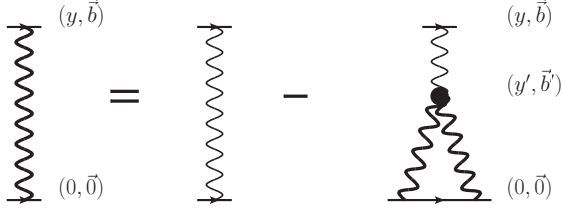


Figure 15: The graphic form of the equation that sums ‘fan’ diagrams. The Green’s function of the exact Pomeron is depicted as bold wavy line, while the ‘bare’ Pomeron is shown by thin wavy line.

We know how to include the impact parameter dependence in the generating function formalism, Eq. (2.8) should be replaced by a new equation [48], which has the following form

$$\boxed{\text{eqpom}} \quad \frac{\partial Z(Y - Y_0; b; u)}{\partial Y} = \alpha'_P \nabla_b^2 Z(Y - Y_0; b; u) - \Delta u(1 - u) Z(Y - Y_0; b; u). \quad (5.1)$$

this sum is the solution of the simple equation shown in Fig. 15, and it is of the form

$$G(y; b) = G_0(y, b) - G_{3P} \int_0^y dy' \int d^2 b' G_0(y - y', \vec{b} - \vec{b}') G^2(y' - 0, \vec{b}'). \quad (5.2) \quad \boxed{\text{COR2}}$$

$G_0(y, b)$ is the Green’s function of the ‘bare’ Pomeron

$$G_0(y, b) = \frac{1}{4\pi\alpha'_P y} e^{\Delta y - \frac{b^2}{4\alpha'_P y}} \xrightarrow{\alpha' \rightarrow 0} \delta^{(2)}(b), \quad (5.3) \quad \boxed{\text{COR3}}$$

which is the Fourier transform of $G(y, q) = \exp(\Delta y - \alpha'_P q^2)$, where $q^2 = -t$ is the momentum transfer squared. G_0 satisfies the equation

$$\frac{\partial G_0(y, b)}{\partial y} - \alpha'_P \nabla_b^2 G_0(y, b) = \Delta G_0(y, b). \quad (5.4) \quad \boxed{\text{COR4}}$$

Using Eq. (5.4), Eq. (5.2) can be rewritten in the form

$$\frac{\partial G(y, b)}{\partial y} - \alpha'_P \nabla_b^2 G(y, b) = \Delta G(y, b) - \Delta G^2(y, b), \quad (5.5)$$

where we substitute $G_{3P} = \Delta$ as in Eq. (2.8).

This equation is the same as Eq. (5.1) for the generating function. Therefore, in the framework of the MPSI approximation Eq. (5.1), together with the obvious property of

$$G_0(y, b) = \int d^2 b' G_0(y - y', \vec{b} - \vec{b}') G_0(y', \vec{b}'), \quad (5.6) \quad \boxed{\text{COR6}}$$

lead to the Green’s function of the exact Pomeron that includes the impact parameter dependence.

As we have discussed, the solution to Eq. (2.8) can be found in the form $Z(G_0(y) f(u))$ in which $f(u)$ that follows from the equation, and the form of Z stems from the initial condition $Z(y = 0, u) = u$. The solution is

$$Z(y, u) = \frac{u}{u + (1 - u) G_0(y)}. \quad (5.7) \quad \boxed{\text{COR7}}$$

We suggest that the solution of Eq. (5.1) has the same form as Eq. (5.7), namely,

$$Z(y, u; b) = \frac{u}{u + (1 - u) G_0(y; b)}. \quad (5.8) \quad \text{COR8}$$

One can see that this form of $Z(y, u; b)$ satisfies the initial condition $Z(y = 0, u; b) = u \delta^{(2)}(\vec{b})$ and $Z(y, u = 1; b) = 1$. Inserting Eq. (5.8) one sees that it does not satisfy Eq. (5.1). We consider

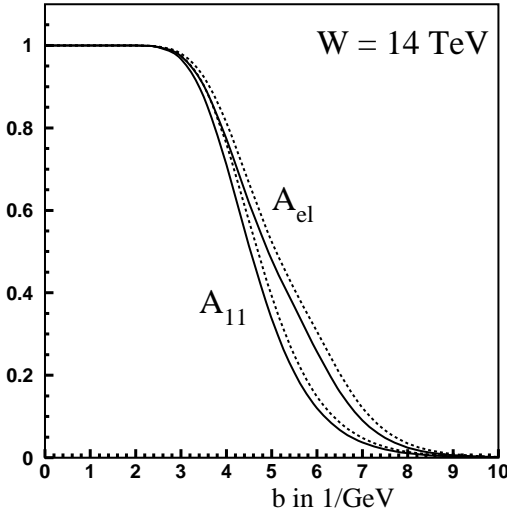


Figure 16: The scattering amplitude A_{11} and A_{el} for $\alpha'_P = 0$ (solid lines) and $\alpha'_P = 0.01 \text{ 1/GeV}^2$ (dashed lines). All other parameters are taken from Ref. [7].

$$\frac{\partial Z(Y - Y_0; b; u)}{\partial Y} = \quad (5.9) \quad \text{COR9}$$

$$\alpha'_P \nabla_b^2 Z(Y - Y_0; b; u) + \Delta u (1 - u) Z(Y - Y_0; b; u) = \frac{b^2}{4 \alpha_P'^2 y^2} G_0^2(y, b) \frac{d^2 Z(G_0(y, b); u)}{(dG_0)^2} \propto \frac{b^2}{4 \alpha_P'^2 y^2} G_0^{-1}.$$

From Eq. (5.9) we see that if $b^2 < (\alpha'_P y)^2$, the corrections are small. Recall that the Pomeron contribution is dominant at $b^2 \leq 4 \alpha'_P y$. It is also small at large values of y since $G_0 \gg 1$.

Having Eq. (5.8) as the solution for the generating function, we can find the exact Green function ($G(y, b)$) for the Pomeron in the MPSI approximation which is equal to Eq. (5.13) with

$$T(Y) \longrightarrow T(Y; b) = \quad (5.10)$$

$$= \gamma G_0(y, b) = \gamma \frac{1}{4\pi \alpha'_P y} e^{\Delta y - \frac{b^2}{4 \alpha_P'^2 y}}.$$

Instead of Eq. (5.15) for Ω_{ik} we have

$$\Omega_{ik}(y, b) = \int d^2 b' \tilde{g}_i, \tilde{g}_k S_{ik}(b') G(y, \vec{b} - \vec{b}'). \quad (5.11) \quad \text{COR11}$$

In Fig. 16 we plot the b space amplitudes for the highest LHC energy with $\alpha'_P = 0$ and $\alpha'_P = 0.01 \text{ GeV}^{-2}$. The difference is negligibly small and, therefore, we neglect the restriction on the kinematic region that followed from taking $\alpha'_P = 0$ (see Eq. (3.16) and Eq. (3.17)). Note, our formalism (due to the MPSI approximation) is only valid for $W \leq 100 \text{ TeV}$ [7], this is far beyond the LHC energy range.

Eq. (5.2) shows that a method to include the energy behaviour of the ‘bare’ Pomeron, is different from the one for a Regge pole. As we have mentioned in N=4 SYM the leading singularity in the angular momentum plane is not a pole but a fixed cut, with an energy behaviour

$$G_0(y, b) \propto y^{-j_0} e^{\Delta y} \quad (5.12) \quad \text{COR12}$$

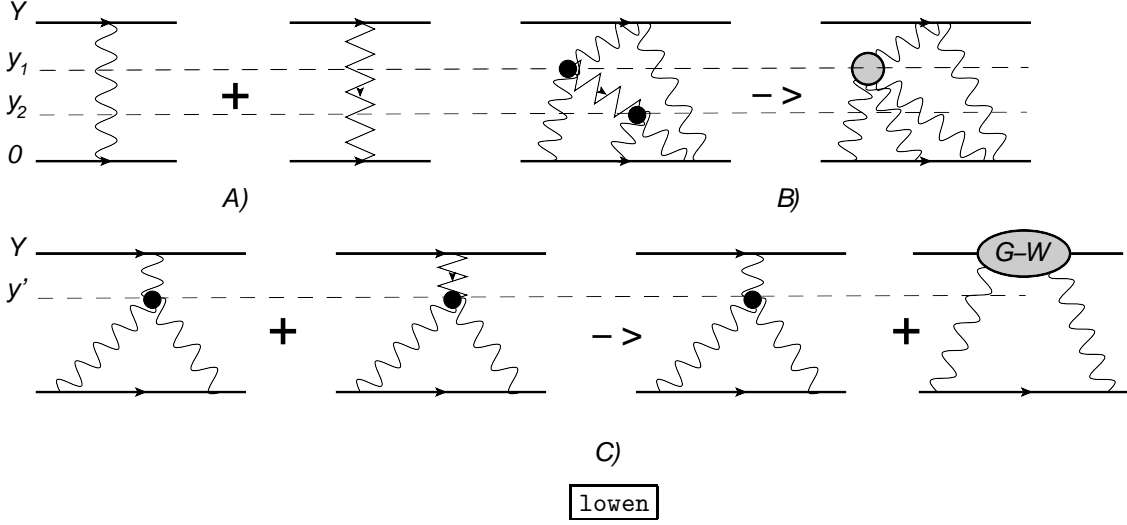


Figure 17: Contributions of secondary Reggeons denoted by zigzag lines. Wavy lines denote the Pomeron. Fig. 17-A shows the contribution to the scattering amplitude due to exchange of a Pomeron and Reggeon. Fig. 17-B and Fig. 17-C illustrates the fact that the exchange of secondary Reggeons can be reduced to the inclusion of the vertices for Pomeron-Pomeron interactions, or can be included in the Good-Walker mechanism.

which satisfies the equation

$$\frac{\partial G_0(y, b)}{\partial y} = \Delta G_0(y, b) - j_0/y G_0(y, b) \rightarrow \Delta G_0(y, b) \quad (5.13) \quad \text{COR13}$$

From Eq. (5.13) one can see that we can neglect the contribution of the factor, y^{-j_0} by differentiating over y . Therefore, Eq. (5.2) can be reduced to Eq. (5.5) which has solution of Eq. (5.8) with G_0 from Eq. (5.12).

5.2 Low energy description and the ‘threshold effect’.

5.2.1 Low energy behaviour of the scattering amplitude

As we shall see in the next section, most of our data base consists of lower energy points from ISR and Sp \bar{p} S/Sp p S ($W \approx 20 - 70$ GeV), where the contribution of the secondary Regge exchanges are important. A secondary Reggeon has an energy behaviour $\exp(\Delta_{\mathcal{R}}(Y - 0))$. The sum $\mathcal{P} + \mathcal{R}$ describes the energy behaviour of the elastic scattering amplitude without screening corrections. This sum replaces the single Pomeron exchange in the definition of Ω_{ik} . Inserting this sum everywhere in the more complicated diagram (see Fig. 17), one can see that the integrations over rapidities reduces the contributions of the secondary Reggeons. By introducing new vertices for the Pomeron-Pomeron interactions (see Fig. 17-B) the integration over $y_1 - y_2$ can be replaced by a new $\mathcal{P} \rightarrow 3\mathcal{P}$ vertex), or it can be absorbed into G-W mechanism (see Fig. 17-C). Since in our approach the vertices, other than the triple Pomeron vertex are considered to

be small, we arrive at the conclusion that for lower energies we only need to replace the single Pomeron exchange by $P + R$, in the definition of Ω_{ik} .

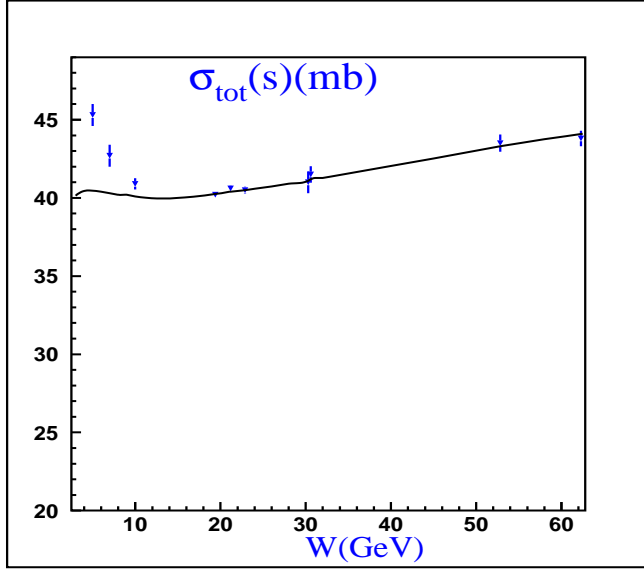


Figure 18: The total cross section ($\sigma_{tot} = 1/2(\sigma_{tot}(pp) + \sigma_{tot}(p\bar{p}))$) at low energies in the framework of our approach with the parameters determined by high energy data. The curve illustrates our parametrization.

well as $y_2 > y_0$. We obtain

$$A(\text{Fig. 4})^{\text{enh1}} = \frac{\tilde{g}^2 \gamma^2}{\Delta^2} e^{-2\Delta(Y-y_0)} + \mathcal{O}(\gamma e^{-\Delta Y}). \quad (5.14) \quad \boxed{\text{TE1}}$$

First, we would like to draw the readers attention to the fact, that without a cutoff the typical $Y - y_1 \approx 1/\Delta$ and $y_2 \approx 1/\Delta$. Therefore, we need to introduce a cutoff only if $y_0 > 1/\Delta$. Second, we need to change $\gamma \rightarrow \gamma \exp(\Delta y_0)$ and multiply the Pomeron exchange by $\Theta(Y - y_0)$. Doing so in our parametrization we obtain the following values for $\langle |S_{enh}^2| \rangle$ for $y_0 = 0, 1.5, 2.3$. For the Tevatron energy ($W = 1.8 \text{ TeV}$) we obtain 0.285, 0.7, 0.99. For LHC ($W = 14 \text{ TeV}$) the corresponding values for $\langle |S_{enh}^2| \rangle$ are 0.06, 0.12, 0.19. $\langle |S_{enh}^2| \rangle$ is the survival probability initiated by the Pomeron interactions. The conclusion from this exercise is very simple: in our approach we do not need to introduce a threshold for Pomeron exchange.

In Fig. 18 we compare our prediction for lower energies with the experimental data and obtain a satisfactory description to within 10%. The conclusion is very simple: we do not need an additional source to describe the lower energy behaviour of the amplitude.

5.2.2 The ‘threshold’ effect

As a consequence of the above conclusion there is no requirement to introduce a Pomeron threshold. i.e. we do not need to assume that the Pomeron contributes to the scattering amplitude for $Y > y_0$ with $y_0 \approx 1.5 \div 2.5$.

Nevertheless, it is interesting to estimate the influence of the threshold cutoff on the value of the scattering amplitude, and especially on the value of the survival probability. We calculate the simplest enhanced diagram of Fig. 4 introducing this cutoff, assuming that $Y - y_1 > y_0$ as

6. The fit to the data and its phenomenology

6.1 The main formulae of the fit

The main formulae, that we use, have been given in sections 4.1 (Eq. ^{FSE91}(4.12)) and 4.2 (Eq. ^{SDF}(4.27), Eq. ^{FSSDGW}(4.29), Eq. ^{FSSDLM}(4.30) and Eq. ^{FSD4}(4.34)). However, we change these formulae so as to take into account the enhanced diagrams. As has been discussed in section 4.1 this procedure reduces to the following substitution in our basic formulae:

$$\begin{aligned} T(Y) \text{ (Eq. ^{ES11}(3.14))} &\longrightarrow G(T(Y)) \text{ (Eq. ^{ES1}(3.13))}; \\ T_{SD}(Y; Y_m) \text{ (Eq. ^{TSD}(4.28))} &\longrightarrow \frac{1}{\gamma} G(T(Y_m)) G(T(Y - Y_m)); \end{aligned} \quad (6.1)$$

We also prefer to use g_i and G_{3P} , instead of \tilde{g}_i and γ in the main formulae of Eq. ^{FSE91}(4.12), considering only $G(T(Y))$ as a function of γ . Finally, this formula has the form

$$A_{i,k}(Y; b) = 1 - \exp \left\{ -\frac{1}{2} \Omega_{IP}^{i,k}(Y; b) \right\} \quad (6.2) \quad \boxed{\text{FIO}}$$

$$\Omega_{IP}^{i,k}(Y; b) = \int d^2 b' \frac{g_i(\vec{b}') g_k(\vec{b} - \vec{b}') (1/\gamma G(T(Y)))}{1 + (G_{3P}/\gamma) G(T(Y)) [g_i(\vec{b}') + g_k(\vec{b} - \vec{b}')] } \quad (6.3) \quad \boxed{\text{FIMF}}$$

Note that g_i in Eq. ^{FIMF}(6.3) have dimension of inverse momentum (see Eq. ^S(2.19)) as well as G_{3P} , while γ is dimensionless. Actually $\gamma^2 = \int d^2 k G_{3P}^2$, but because we do not know the dependence of G_{3P} with respect to transverse momenta of Pomerons, we consider γ and G_{3P} as independent parameters of the fit.

In Eq. ^{SDF}(4.27) we have to replace all \tilde{g}_i by g_i and multiply it by factor G_{3P}/γ^2 in addition to the substitution of Eq. ^{F11}(6.1).

For completeness of presentation we list below the formulae for physical observables (see Re. [7] for details). The amplitudes for the observable processes have the form

$$a_{el}(s, b) = i\{\alpha^4 A_{1,1} + 2\alpha^2 \beta^2 A_{1,2} + \beta^4 A_{2,2}\}, \quad (6.4) \quad \boxed{\text{EL}}$$

$$a_{sd}(s, b) = i\alpha\beta\{-\alpha^2 A_{1,1} + (\alpha^2 - \beta^2) A_{1,2} + \beta^2 A_{2,2}\}, \quad (6.5) \quad \boxed{\text{SD}}$$

$$a_{dd}(s, b) = i\alpha^2 \beta^2 \{A_{1,1} - 2A_{1,2} + A_{2,2}\}. \quad (6.6) \quad \boxed{\text{DD}}$$

,

The corresponding cross sections are given by

$$\sigma_{tot}(s) = 2 \int d^2 b a_{el}(s, b), \quad (6.7) \quad \boxed{\text{XST}}$$

$$\sigma_{el}(s) = \int d^2 b |a_{el}(s, b)|^2, \quad (6.8) \quad \boxed{\text{XSEL}}$$

$$\sigma_{sd}(s) = \int d^2 b |a_{sd}(s, b)|^2, \quad (6.9) \quad \boxed{\text{XSSD}}$$

$$\sigma_{dd}(s) = \int d^2 b |a_{dd}(s, b)|^2. \quad (6.10) \quad \boxed{\text{XSDD}}$$

6.2 The strategy of our fitting procedure

Our Pomeron model, as well as the KMR [9] and Ostapchenko [10] models have the same following ingredients:

- 1) A bare non-screened Pomeron exchange amplitude.
- 2) s-channel unitarity is enforced by eikonal rescatterings of the colliding projectiles.
- 3) These rescatterings proceed through elastic and diffractive states according to the G-W mechanism.
- 4) t-channel unitarity is maintained through the Pomeron interactions.

In our model the Pomeron is specified by nine parameters, the Tevatron data on its own is not sufficient to determine the parameters. Consequently, we have also to include ISR - SP \bar{p} S/SppS lower energy ($W \approx 20-70$ GeV) data. This data has small errors which facilitate a reasonably reliable fit. To reduce the number of Reggeon parameters, we define $\sigma_{tot} = \frac{1}{2}(\sigma_{tot}(pp) + \sigma_{tot}(p\bar{p}))$. The inclusion of the Regge sector of our fit requires five additional parameters. i.e. we have fourteen parameters in all.

Our data base has 58 experimental data points, which include the p-p and \bar{p} -p total cross sections, integrated elastic cross sections, integrated single and double diffraction cross sections, B_{el} , to which we have added a consistency check of the CDF data $\frac{d\sigma_{el}}{dt}$ ($-t \leq 0.5 \text{ GeV}^2$), $\frac{d^2\sigma_{sd}}{dt dM^2/s}$ ($t = 0.05 \text{ GeV}^2$) and B_{sd} .

The data points were fitted to determine the 14 free parameters of our model. We fit simultaneously the entire data base. The only minor tuning which we employ is discussed in section 6.2.

As was mentioned in the previous section, most of the experimental data is available at low energies ($\sqrt{s} \approx 20 - 70 \text{ GeV}$) where the secondary Reggeon contributions are essential. this data has small errors. We deal with the secondary reggeon in the same way as in Ref. [7] adding Ω_R to Ω_P in Eq. (6.2).

Using the parameters of the fit (see Table 1), we find that the contributions of the large mass diffraction to the single diffractive cross section as well as to the double diffractive cross section, are rather small. Therefore, we neglect these contributions and use Eq. (4.29) and Eq. (4.33) in the fit. After determining the parameters of the fit we use them to describe the large mass diffraction.

6.3 The results of the fit

As stated above, our fit is based on 58 experimental data points. The model gives a good reproduction of the data, with a $\chi^2/d.o.f. = 1.56$. However, a large contribution to the value of $\chi^2/d.o.f.$ stems from the uncertainty of the value of two single diffraction cross sections, and of the CDF total cross section [57] at the Tevatron ($W = 1800 \text{ GeV}$). Neglecting the contribution of these three points to the total χ^2 we obtain $\chi^2/d.o.f. = 0.86$. The quality of the description of the experimental data is demonstrated in Fig. 19. The values of fitted parameters are listed in Table 1. An important advantage of our fit is that it provides a good reproduction of σ_{dd} .

In Fig. 20 the amplitudes A_{ik} are plotted. One can see that in spite of the smallness of α'_P we reproduce the growth of the radius of interaction with energy. The values of physical observables for higher energies are shown in Table 2.

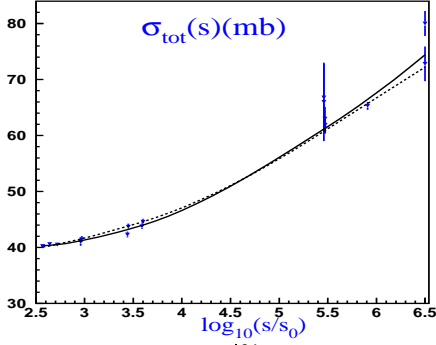


Fig. 19-a

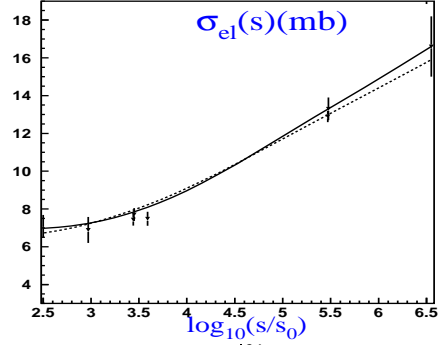


Fig. 19-b

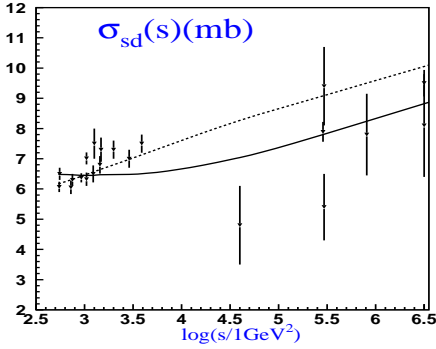


Fig. 19-c

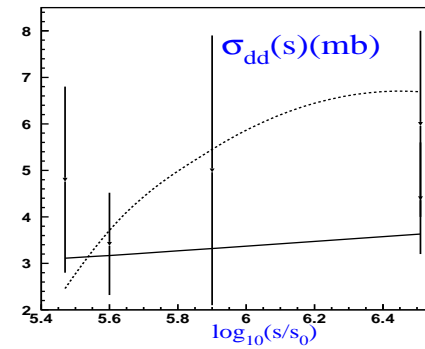


Fig. 19-d

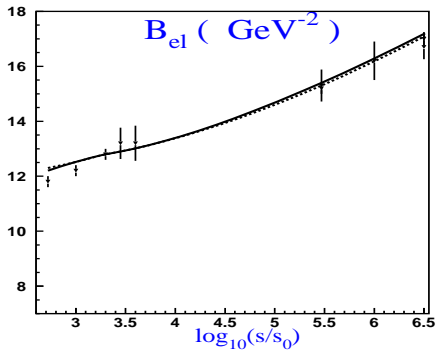


Fig. 19-e

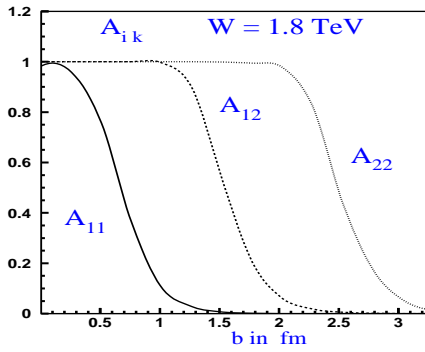


Fig. 19-f

Figure 19: Comparison with the experimental data the energy behaviour of the total (Fig. 19-a), elastic (Fig. 19-b), single diffraction (Fig. 19-c) and double diffraction (Fig. 19-d) cross sections and elastic slope (Fig. 19-e). The solid lines show this fit while the dashed lines correspond to the fit of Ref. [7]. Fig. 19-f shows the behaviour of the amplitude $A_{i,k}$ as function of the impact parameter b for the Tevatron energy.

6.4 Comments on the parameter values of the fit

An attractive feature of our fit is that the exceedingly small value of $\alpha'_{\mathcal{P}}$ found in the original fit [7] is

Δ_P	β	α'_P	g_1	g_2	m_1	m_2
0.2	0.388	0.020 GeV^{-2}	2.53 GeV^{-1}	88.4 GeV^{-1}	2.648 GeV	1.37 GeV
Δ_R	γ	α'_R	g_1^R	g_2^R	$R_{0,1}^2$	G_{3P}
-0.466	0.0033	0.4 GeV^{-2}	14.5 GeV^{-1}	1343 GeV^{-1}	4.0 GeV^{-2}	0.0173 GeV^{-1}

t1

Table 1: Fitted parameters for our model. The quality of the fit is $\chi^2/d.o.f. = 0.86$ (see the detailed explanation in the text)

reproduced. However, the values obtained for Δ_P and γ are smaller than our previous values [7]). Our results suggest that the complete summation of the Pomeron interaction sector, presented in this paper, induces a weaker screening that was found by the partial summation presented in Ref. [7]. A consequence of this feature is that S_{enh}^2 calculated in this paper is expected to be larger than the corresponding values obtained in [7] .

The small value obtained for $\gamma = 0.0033$ is encouraging, since $\gamma \propto \alpha_s^2$ in QCD, supports our key supposition that rather short distances, contribute to the soft interaction at high energy, in agreement with all approaches to the Pomeron structure considered above. Note, that since $\gamma^2 = \int d^2k G_{3P}^2$ we can evaluate the value of the typical transverse momentum of the Pomeron in the triple Pomeron vertex, which turns out to be $\approx 1 \text{ GeV}$.

g_2 is rather large, as in our previous approaches (see Ref. [7]). The consequence of $\frac{g_2}{g_1} \gg 1$ is seen in Fig. 19-f, where the amplitude $A_{i,k}$ are shown at the Tevatron energy. One can see that amplitude A_{22} is equal to one in a wide region of b and, therefore, corresponds to black disc scattering. However, its contribution is proportional to β^4 in elastic amplitude and to β^2 in single and double diffraction amplitudes, consequently, it's relative contribution is small.

It should be stressed that the value of our phenomenological parameters (see Table 1) are in agreement with the theoretical estimates of Eq. (2.18). Choosing the typical soft scale $\mu = 1 \text{ GeV}$ we can see that $g_i \mu \approx 1$ and

$$G_{3P} \mu \approx \gamma \approx \Delta_P^2 \ll \Delta_P \ll g_i \mu \quad (6.11) \quad \text{FI3}$$

As we have discussed, in this paper we sum all diagrams in an approximation in which $g_i G(T(Y)) \geq 1$ while $\Delta_P^2 G(T(Y)) \ll 1$. The values of the fit parameters support the use of the approximation.

In Fig. 20 the amplitudes A_{ik} are plotted.

The values of physical observables for higher energies are shown in Table 2.

6.5 Comparison with other approaches.

At present there are three groups that are working on modelling the strong interaction at high energies: Durham group [9], Ostapchenko [10] and our group. The models have a lot in common: a rather large value of Δ_P , small values of α'_P , a large contribution of the Good-Walker mechanism, and a significant Pomeron-Pomeron interaction. The theories mainly differ in the way the Pomeron-Pomeron interaction

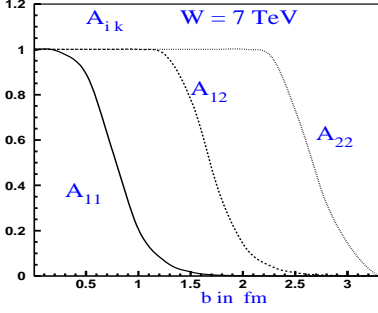


Fig. 20-a

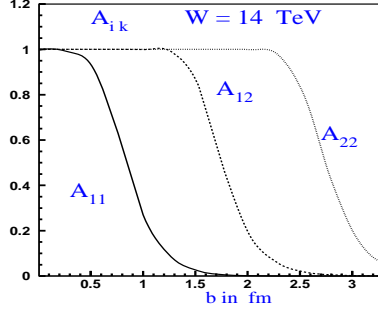


Fig. 20-b

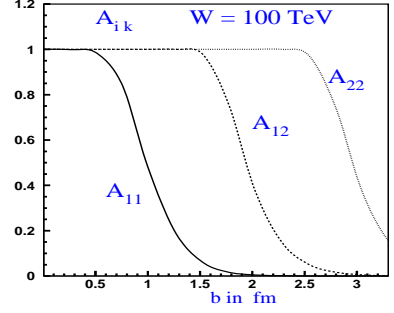


Fig. 20-c

Figure 20: The amplitudes A_{ik} versus b at LHC energies.

W(TeV)	$\sigma_{tot}(mb)$	$\sigma_{el}(mb)$	$\sigma_{sd}(mb)$	$\sigma_{dd}(mb)$	$B_{el}(GeV^{-1})$
0.9	66.3	15	8.24	3.83	16.1
1.8	74.4	17.5	8.87	4.46	17.2
2.3	77.3	18.4	9.1	4.59	17.5
3.5	82.5	20.1	9.49	4.72	18.2
5	87	21.6	9.83	5.59	18.8
7	91.3	23	10.2	6.46	19.3
10	96	24.6	10.5	6.48	19.9
14	101	26.1	10.8	6.5	20.5
100	128	35.6	12.7	7.79	29.9

Table 2: Predictions for energies that will be accessible at the LHC.

is taken into account. In the Durham model as well as in the Ostapchenko one, all vertices of Pomeron-Pomeron interactions are included, using a slightly different phenomenological ansatz. In our model we include only the triple Pomeron vertex, as has been discussed in section 1. In the Durham and in our models $\Delta_P \approx 0.2 \div 0.3$ and $\alpha'_P \approx 0$, while the Ostapchenko model gives $\Delta_P = 0.14$ and $\alpha'_P = 0.14 GeV^{-1}$. All models give more or less the same results at the Tevatron energy, and their results at the highest LHC energy: span the values $\sigma_{tot} = 86 \div 114 mb$, $\sigma_{el} = 20 \div 30 mb$, $\sigma_{sd} = 10 \div 16 mb$ and $\sigma_{dd} = 5 \div 13 mb$.

Note that the Ostapchenko model also includes a hard Pomeron, while our model has only a single Pomeron. The KMR model is more complicated as the Pomeron dependence on k_t^2 is described by three Pomerons. As one can see from Table 3, the Ostapchenko model leads to the largest value for the total and elastic cross sections, and gives small values for the double diffractive cross section. The Durham model predicts the lowest value of the total cross section but a rather large double diffraction cross section.

	Tevatron (1.8 TeV)					LHC (14 TeV)				
	GLMM	GLM	KMR(07)	KMR(10)	OS(C)	GLMM	GLM	KMR(07)	KMR(10)	OS(C)
$\sigma_{tot}(\text{mb})$	73.29	74.4	74.0	73.9	73.0	92.1	101	88.0	86.3	114.0
$\sigma_{el}(\text{mb})$	16.3	17.5	16.3	15.1	16.8	20.9	26.1	20.1	18.1	33.0
$\sigma_{sd}(\text{mb})$	9.76	8.87	10.9	12.7	9.6	11.8	10.8	13.3	16.1	11.0
$\sigma_{dd}(\text{mb})$	5.36	3.53	7.2	13.3	3.93	6.1	6.5	13.4	12.9	4.83

Table 3: Comparison with the other models: GLMM is our model in which we summed only enhanced diagrams [7], GLM is the model described in this paper, KMR(07) and KMR(10) are two models of Durham group ((Ref. [9]) and OS(C) is the model developed in Ref. [10]. The predictions of the fit of 2010 is preliminary and are taken from the talk of A.Martin at Diffraction’10.

7. Conclusions

In this paper we have constructed a model to describe strong interactions at high energy, based on two main theoretical criteria: it should include the main result of N=4 SYM, which is the only theory that is able to deal with a large coupling constant; and it should provide the natural matching with high energy QCD. In accord with these ideas we assumed that Δ_P is relatively large and $\alpha'_P \rightarrow 0$. Using these assumptions in this paper we sum all enhanced and semi-enhanced diagrams. The enhanced diagrams have been calculated in our previous paper [7]. For the first time we obtain analytical formulae for the scattering amplitude both for elastic scattering and for diffractive production.

Using these formulae we made a fit to the available experimental data and predict the main soft observables at LHC energies (see Tables 2 and 3).

We study the accuracy of our approach related to the corrections induced by small (both not equal to zero α'_P) and by the fact that the ‘bare’ Pomeron cannot be a Regge pole, but a cut.

In this paper we have completed the formulation of a theoretical self consistent approach. In the future we intend to apply this approach to the numerous practical problems, such as survival probability for di-jet and Higgs production, inclusive cross sections, rapidity and multiplicity correlations.

Acknowledgements

We thank all participants of the conference “Diffraction 2010” for fruitful discussion on the subject. The research of one of us (E.L.) was supported in part by the Fondecyt (Chile) grant # 1100648.

References

- [COL] [1] P.D.B. Collins, *"An introduction to Regge theory and high energy physics"*, Cambridge University Press 1977.
- [SOFT] [2] Luca Caneschi (editor), *"Regge Theory of Low - p_T Hadronic Interaction"*, North-Holland 1989.
- [LEREG] [3] E. Levin, *"An introduction to Pomerons"*, arXiv:hep-ph/9808486; *"Everything about Reggeons. I: Reggeons in *soft* interaction"*, arXiv:hep-ph/9710546.
- [ATMP] [4] V. A. Khoze, A. D. Martin and M. G. Ryskin, Eur. Phys. J. **C18** (2000) 167; Phys. Lett. **B643** (2006) 93; A. B. Kaidalov, V. A. Khoze, A. D. Martin and M. G. Ryskin, Eur. Phys. J. **C31** (2003) 387; **C33** (2004) 261. E. Gotsman, E. Levin and U. Maor, Phys. Lett. **B452** (1999) 387; **B309** (1993) 199; Phys. Rev. **D49** (1994) R4321; A. Capella, U. Sukhatme, C-I Tan *et al.* Phys. Rept. **236**, 225-329 (1994). A. B. Kaidalov, Phys. Rept. **50** (1979) 157; A. B. Kaidalov, L. A. Ponomarev and K. A. Ter-Martirosian, Yad. Fiz. **44** (1986) 722 [Sov. J. Nucl. Phys. **44** (1986) 468]; A. B. Kaidalov and K. A. Ter-Martirosyan, Nucl. Phys. B **75** (1974) 471.
- [2CH] [5] E. Gotsman, E. Levin and U. Maor, Phys. Lett. **B452** (1999) 387; **B309** (1993) 199; Phys. Rev. **D49** (1994) R4321.
- [MLAST] [6] E. Gotsman, E. Levin, U. Maor, Phys. Rev. **D81** (2010) 051501 [arXiv:1001.5157 [hep-ph]]; Braz. J. Phys. **38** (2008) 431-436 [arXiv:0805.0418 [hep-ph]]; *"A Soft Interaction Model at Ultra High Energies: Amplitudes, Cross Sections and Survival Probabilities"*, arXiv:0708.1506 [hep-ph]; E. Gotsman, A. Kormilitzin, E. Levin *et al.*, Eur. Phys. J. **C52** (2007) 295-304 [arXiv:1001.5157 [hep-ph]].
- [GLMM] [7] E. Gotsman, E. Levin, U. Maor and J. S. Miller, Eur. Phys. J. **C57** (2008) 689-709. [arXiv:0805.2799 [hep-ph]].
- [GLMA] [8] E. Gotsman, A. Kormilitzin, E. Levin and U. Maor, Nucl. Phys. A **842** (2010) 82 [arXiv:0912.4689 [hep-ph]].
- [KMRS] [9] M. G. Ryskin, A. D. Martin, V. A. Khoze *et al.*, J. Phys. G **G36** (2009) 093001 [arXiv:0907.1374 [hep-ph]]; Eur. Phys. J. **C60** (2009) 265-272. [arXiv:0812.2413 [hep-ph]]; Eur. Phys. J. **C60** (2009) 249-264. [arXiv:0812.2407 [hep-ph]]; AIP Conf. Proc. **1105** (2009) 252-257. [arXiv:0811.1481 [hep-ph]]; *"Soft Diffraction at the LHC,"* arXiv:0810.3324 [hep-ph]; *"Rapidity gap survival probability and total cross sections,"* arXiv:0810.3560 [hep-ph]; Eur. Phys. J. **C54** (2008) 199 [arXiv:0710.2494 [hep-ph]].
- [OS] [10] S. Ostapchenko, Phys. Rev. D **81** (2010) 114028 [arXiv:1003.0196 [hep-ph]]; Phys. Rev. D **77** (2008) 034009 [arXiv:hep-ph/0612175]; Phys. Lett. B **636** (2006) 40 [arXiv:hep-ph/0602139].
- [S-CFT] [11] J. M. Maldacena, Adv. Theor. Math. Phys. **2** (1998) 231 [Int. J. Theor. Phys. **38** (1999) 1113] [arXiv:hep-th/9711200]; S. S. Gubser, I. R. Klebanov and A. M. Polyakov, Phys. Lett. B **428** (1998) 105 [arXiv:hep-th/9802109]; E. Witten, Adv. Theor. Math. Phys. **2** (1998) 505 [arXiv:hep-th/9803131].
- [POST] [12] J. Polchinski and M. J. Strassler, JHEP **0305** (2003) 012 [arXiv:hep-th/0209211]; Phys. Rev. Lett. **88** (2002) 031601 [arXiv:hep-th/0109174].
- [BFL4] [13] A. V. Kotikov, L. N. Lipatov, A. I. Onishchenko and V. N. Velizhanin, Phys. Lett. B **595** (2004) 521 [Erratum-ibid. B **632** (2006) 754] [arXiv:hep-th/0404092]; A. V. Kotikov and L. N. Lipatov, Nucl. Phys. B **661** (2003) 19 [Erratum-ibid. B **685** (2004) 405] [arXiv:hep-ph/0208220]; A. V. Kotikov and L. N. Lipatov, Nucl. Phys. B **582** (2000) 19 [arXiv:hep-ph/0004008].
- [BST] [14] R. C. Brower, J. Polchinski, M. J. Strassler and C. I. Tan, JHEP **0712** (2007) 005 [arXiv:hep-th/0603115]; R. C. Brower, M. J. Strassler and C. I. Tan, JHEP **0903** (2009) 092 [arXiv:0710.4378 [hep-th]]; JHEP **0903** (2009) 050. [arXiv:0707.2408 [hep-th]].

- [HIM] [15] Y. Hatta, E. Iancu and A. H. Mueller, JHEP **0801** (2008) 026 [arXiv:0710.2148 [hep-th]].
- [COCO] [16] L. Cornalba and M. S. Costa, Phys. Rev. **D 78**, (2008) 09010, arXiv:0804.1562 [hep-ph]; L. Cornalba, M. S. Costa and J. Penedones, JHEP **0806** (2008) 048 [arXiv:0801.3002 [hep-th]].
- [BEPI] [17] B. Pire, C. Roiesnel, L. Szymanowski and S. Wallon, Phys. Lett. B **670**, 84 (2008) [arXiv:0805.4346 [hep-ph]].
- [LMKS] [18] E. Levin, J. Miller, B. Z. Kopeliovich and I. Schmidt, JHEP **0902**, 048 (2009) [arXiv:0811.3586 [hep-ph]].
- [FEYN] [19] R. P. Feynman, Phys. Rev. Lett. **23** (1969) 1415; *"Photon-Hadron Interactions"*, Reading 1972, p282
- [GRIB] [20] V. N. Gribov, *"Space-time description of hadron interactions at high energies"*, arXiv:hep-ph/0006158; Sov. J. Nucl. Phys. **9** (1969) 369 [Yad. Fiz. **9** (1969) 640].
- [BJ] [21] J. D. Bjorken and E. A. Paschos, Phys. Rev. **185**, (1969) 1975.
- [LONU] [22] F. E. Low, Phys. Rev. **D12** (1975) 163. S. Nussinov, Phys. Rev. Lett. **34** (1975) 1286.
- [BFLK] [23] E. A. Kuraev, L. N. Lipatov, and F. S. Fadin, Sov. Phys. JETP **45**, 199 (1977); Ya. Ya. Balitsky and L. N. Lipatov, Sov. J. Nucl. Phys. **28**, 22 (1978).
- [LI] [24] L. N. Lipatov, Phys. Rep. **286** (1997) 131; Sov. Phys. JETP **63** (1986) 904 and references therein.
- [GLR] [25] L. V. Gribov, E. M. Levin and M. G. Ryskin, Phys. Rep. **100** (1983) 1.
- [MUQI] [26] A. H. Mueller and J. Qiu, Nucl. Phys. **B268** (1986) 427.
- [MV] [27] L. McLerran and R. Venugopalan, Phys. Rev. **D49** (1994) 2233, 3352; **D50** (1994) 2225; **D53** (1996) 458; **D59** (1999) 09400.
- [B] [28] I. Balitsky, [arXiv:hep-ph/9509348]; Phys. Rev. **D60**, 014020 (1999) [arXiv:hep-ph/9812311]
- [K] [29] Y. V. Kovchegov, Phys. Rev. **D60**, 034008 (1999), [arXiv:hep-ph/9901281].
- [IMWLK] [30] J. Jalilian-Marian, A. Kovner, A. Leonidov and H. Weigert, Phys. Rev. **D59**, 014014 (1999), [arXiv:hep-ph/9706377]; Nucl. Phys. **B504**, 415 (1997), [arXiv:hep-ph/9701284]; J. Jalilian-Marian, A. Kovner and H. Weigert, Phys. Rev. **D59**, 014015 (1999), [arXiv:hep-ph/9709432]; A. Kovner, J. G. Milhano and H. Weigert, Phys. Rev. **D62**, 114005 (2000), [arXiv:hep-ph/0004014]; E. Iancu, A. Leonidov and L. D. McLerran, Phys. Lett. **B510**, 133 (2001); [arXiv:hep-ph/0102009]; Nucl. Phys. **A692**, 583 (2001), [arXiv:hep-ph/0011241]; E. Ferreira, E. Iancu, A. Leonidov and L. McLerran, Nucl. Phys. **A703**, 489 (2002), [arXiv:hep-ph/0109115]; H. Weigert, Nucl. Phys. **A703**, 823 (2002), [arXiv:hep-ph/0004044].
- [BRN] [31] M. A. Braun, Phys. Lett. **B632** (2006) 297 [arXiv:hep-ph/0512057]; Eur. Phys. J. **C16** (2000) 337 [arXiv:hep-ph/0001268]; Phys. Lett. **B483** (2000) 115 [arXiv:hep-ph/0003004]; Eur. Phys. J. **C33** (2004) 113 [arXiv:hep-ph/0309293]; **C6**, 321 (1999) [arXiv:hep-ph/9706373]. M. A. Braun and G. P. Vacca, Eur. Phys. J. **C6** (1999) 147 [arXiv:hep-ph/9711486].
- [BART] [32] J. Bartels, M. Braun and G. P. Vacca, Eur. Phys. J. **C40** (2005) 419 [arXiv:hep-ph/0412218]. J. Bartels and C. Ewerz, JHEP **9909** 026 (1999) [arXiv:hep-ph/9908454]. J. Bartels and M. Wusthoff, Z. Phys. **C6**, (1995) 157. A. H. Mueller and B. Patel, Nucl. Phys. **B425** (1994) 471 [arXiv:hep-ph/9403256]. J. Bartels, Z. Phys. **C60** (1993) 471.
- [LEPO] [33] E. Levin and I. Potashnikova, JHEP **1008** (2010) 112; [arXiv:1007.0306 [hep-ph]].
- [MUCD] [34] A. H. Mueller, Nucl. Phys. **B415** (1994) 373; **B437** (1995) 107.

- [LAE] [35] E. Laenen and E. Levin, Nucl. Phys. **B451** (1995) 207.
- [LELU] [36] E. Levin and M. Lublinsky, Nucl. Phys. A **763** (2005) 172 [arXiv:hep-ph/0501173]; Phys. Lett. B **607** (2005) 131 [arXiv:hep-ph/0411121]; Nucl. Phys. A **730** (2004) 191 [arXiv:hep-ph/0308279].
- [KLP] [37] M. Kozlov, E. Levin and A. Prygarin, Nucl. Phys. **A792** (2007) 122 [arXiv:0704.2124 [hep-ph]].
- [LT] [38] E. Levin and K. Tuchin, Nucl. Phys. **A693** (2001) 787 [arXiv:hep-ph/0101275]; **A691** (2001) 779 [arXiv:hep-ph/0012167]; **B573** (2000) 833 [arXiv:hep-ph/9908317].
- [NS] [39] N. Armesto and M. A. Braun, Eur. Phys. J. **C20**, 517 (2001) [arXiv:hep-ph/0104038]; M. Lublinsky, Eur. Phys. J. **C21**, 513 (2001) [arXiv:hep-ph/0106112]; E. Levin and M. Lublinsky, Nucl. Phys. **A712**, 95 (2002) [arXiv:hep-ph/0207374]; Nucl. Phys. **A712**, 95 (2002) [arXiv:hep-ph/0207374]; Eur. Phys. J. **C22**, 647 (2002) [arXiv:hep-ph/0108239]; M. Lublinsky, E. Gotsman, E. Levin and U. Maor, Nucl. Phys. **A696**, 851 (2001) [arXiv:hep-ph/0102321]; Eur. Phys. J. **C27**, 411 (2003) [arXiv:hep-ph/0209074]; K. Golec-Biernat, L. Motyka and A. Stasto, Phys. Rev. **D65**, 074037 (2002) [arXiv:hep-ph/0110325]; E. Iancu, K. Itakura and S. Munier, Phys. Lett. **B590** (2004) 199 [arXiv:hep-ph/0310338]. K. Rummukainen and H. Weigert, Nucl. Phys. **A739**, 183 (2004) [arXiv:hep-ph/0309306]; K. Golec-Biernat and A. M. Stasto, Nucl. Phys. **B668**, 345 (2003) [arXiv:hep-ph/0306279]; E. Gotsman, M. Kozlov, E. Levin, U. Maor and E. Naftali, Nucl. Phys. **A742**, 55 (2004) [arXiv:hep-ph/0401021]; K. Kutak and A. M. Stasto, Eur. Phys. J. **C41**, 343 (2005) [arXiv:hep-ph/0408117]; G. Chachamis, M. Lublinsky and A. Sabio Vera, Nucl. Phys. **A748**, 649 (2005) [arXiv:hep-ph/0408333]; J. L. Albacete, N. Armesto, J. G. Milhano, C. A. Salgado and U. A. Wiedemann, Phys. Rev. **D71**, 014003 (2005) [arXiv:hep-ph/0408216]; E. Gotsman, E. Levin, U. Maor and E. Naftali, Nucl. Phys. **A750** (2005) 391 [arXiv:hep-ph/0411242]; Y. V. Kovchegov, J. Kuokkanen, K. Rummukainen and H. Weigert, Nucl. Phys. **A823** (2009) 47-82. [arXiv:0812.3238 [hep-ph]]; J. L. Albacete, N. Armesto, J. G. Milhano and C. A. Salgado, Phys. Rev. **D80** (2009) 034031. [arXiv:0902.1112 [hep-ph]].
- [BALE] [40] J. Bartels and E. Levin, Nucl. Phys. **B387** (1992) 617.
- [KHLE] [41] D. Kharzeev and E. Levin, Nucl. Phys. B **578** (2000) 351 [arXiv:hep-ph/9912216].
- [KKL] [42] D. E. Kharzeev, Y. V. Kovchegov and E. Levin, Nucl. Phys. A **690** (2001) 621 [arXiv:hep-ph/0007182].
- [DL] [43] A. Donnachie and P.V. Landshoff, Nucl. Phys. **B231**, (1984) 189; Phys. Lett. **B296**, (1992) 227; Zeit. Phys. **C61**, (1994) 139.
- [BMOV] [44] V. N. Gribov, Sov. Phys. JETP **15** (1962) 873 [Zh. Eksp. Teor. Fiz. **42** (1962 NUPHA,40,107.1963) 1260].
- [GW] [45] M. L. Good and W. D. Walker, Phys. Rev. **120** (1960) 1857.
- [RIBRT] [46] V. N. Gribov, Sov. Phys. JETP **26** (1968) 414 [Zh. Eksp. Teor. Fiz. **53** (1967) 654].
- [BORY] [47] K. G. Boreskov, A. B. Kaidalov, V. A. Khoze, A. D. Martin and M. G. Ryskin, Eur. Phys. J. **C44** (2005) 523 [arXiv:hep-ph/0506211].
- [GRPO] [48] P. Grassberger and K. Sundermeyer, Phys. Lett. **B77** (1978) 220. E. Levin, Phys. Rev. **D49** (1994) 4469. K. G. Boreskov, "Probabilistic model of Reggeon field theory", arXiv:hep-ph/0112325 and reference therein.
- [AMCP] [49] D. Amati, M. Le Bellac, G. Marchesini and M. Ciafaloni, Nucl. Phys. **B112** (1976) 107; D. Amati, G. Marchesini, M. Ciafaloni and G. Parisi, Nucl. Phys. **B114** (1976) 483.
- [KOLE] [50] M. Kozlov and E. Levin, Nucl. Phys. A **A779** (2006) 142 [arXiv:hep-ph/0604039].
- [KOLE1] [51] M. Kozlov, E. Levin, V. Khachatryan and J. Miller, Nucl. Phys. A **791** (2007) 382 [arXiv:hep-ph/0610084].

- FROI** [52] M. Froissart, *Phys. Rev.* **123** (1961) 1053;
A. Martin, “Scattering Theory: Unitarity, Analyticity and Crossing.” Lecture Notes in Physics,
Springer-Verlag, Berlin-Heidelberg-New-York, 1969.
- MPSI** [53] A. H. Mueller and B. Patel, Nucl. Phys. **B425** (1994) 471. A. H. Mueller and G. P. Salam, Nucl. Phys. **B475**,
(1996) 293. [arXiv:hep-ph/9605302]. G. P. Salam, Nucl. Phys. **B461** (1996) 512; E. Iancu and A. H. Mueller,
Nucl. Phys. **A730** (2004) 460 [arXiv:hep-ph/0308315]; 494 [arXiv:hep-ph/0309276].
- LEPR** [54] E. Levin and A. Prygarin, Eur. Phys. J. **C53** (2008) 385 [arXiv:hep-ph/0701178].
- LMP** [55] E. Levin, J. Miller and A. Prygarin, E. Levin, J. Miller, A. Prygarin, Nucl. Phys. **A806** (2008) 245-286.
[arXiv:0706.2944 [hep-ph]].
- DG1** [56] A. D. Martin, M. G. Ryskin and V. A. Khoze, “*Forward Physics at the LHC*,” arXiv:0903.2980 [hep-ph].
- CDF** [57] CDF Collaboration, Phys. Rev. **D50** (1994) 5535.
- RY** [58] I. Gradstein and I. Ryzhik, “*Tables of Series, Products, and Integrals*”, Verlag MIR, Moskau, 1981.
- KL** [59] Y. V. Kovchegov and E. Levin, Nucl. Phys. **B577** (2000) 221 [arXiv:hep-ph/9911523].